Micro and Nanosystems, 2020, *12*, 4-22

REVIEW ARTICLE

Superparamagnetic Iron Oxide as Photocatalyst and Adsorbent in Wastewater Treatment – A Review

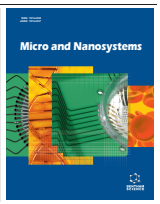

Nur Shazrynda Md. Shahrodin[1,2], Juhana Jaafar[1,2,*], Abdul Razak Rahmat[2], Norhaniza Yusof[1,2], Mohammad Hafiz Dzarfan Othman[1,2] and Mukhlis A. Rahman[1,2]

[1]*Advanced Membrane Technology Research Center, Faculty of Chemical and Energy Engineering, Universiti Teknologi, Johor Bahru, Malaysia;* [2]*School of Chemical and Energy Engineering, Faculty of Chemical Engineering, Universiti Teknologi, Johor Bahru, Malaysia*

ARTICLE HISTORY

Received: April 02, 2019
Revised: May 18, 2019
Accepted: June 24, 2019

DOI:
10.2174/1876402911666190716155658

Abstract: Superparamagnetic iron oxide has been applied in different fields for various reasons. Its abundant availability, non-toxic properties, environmentally friendly and good chemical stability in aqueous medium are beneficial for water treatment applications. In addition, its low bad gap (2.3 ~ 2.4 eV) has contributed to highly possible electrons-holes activation under the visible light spectrum. On the realization of iron oxide capabilities as a promising alternative to conventional anatase TiO_2 photocatalysts, this review is presented to critically discuss the photocatalytic behaviour of organic water pollutants as a function of iron oxide properties. The concluding remarks in terms of the way forward in the opportunities of iron oxide superparamagnetic properties can benefit towards the photocatalytic activities including recycling, retrieving and controlling in wastewater treatment.

Keywords: Superparamagnetic iron oxide, iron oxide photocatalyst, iron oxide adsorbent, Fe_2O_3, Fe_3O_4, waste water treatment.

1. INTRODUCTION

Iron (Fe) is a highly reactive element that can be present in variable oxidation state, which allows it to coordinate with other elements. Iron oxide (IO) exist in a range of chemical and physical forms; FeO ↔ Fe_3O_4 ↔ γ-Fe_2O_3 ↔ α-Fe_2O_3 ↔ FeOOH [1], where the most discussed and common forms are magnetite (Fe_3O_4), hematite (α-Fe_2O_3) and maghemite (γ-Fe_2O_3) due to their nano-range, high surface to volume ratios and superparamagnetism properties [2]. These iron oxides are basically constructed on a close-packed of O^{2-} anion lattice, with smaller Fe cations occupying octahedrally and tetrahedrally coordinated interstices in between [3]. Iron oxide semiconductor possesses a unique magnetism characteristic; superparamagnetism [4]. Superparamagnetism allows for controlling, retrieving, and directing processes making it more convenient and efficient [5]. The magnetism arises from the relative electric charge (orbital/spin motion). The fundamental of iron oxide magnetism is the magnetic moment, which attributes to the unpaired electrons in their atomic shells especially in the 3d and 4f shells of each atom (Fig. **1a**). Thus, the magnetic moment of delocalized electrons in the metal and interatomic interactions between localized magnetic moments in molecules can result in magnetic ordering [6]. Superparamagnetic IO nanoparticles have a large constant magnetic moment and behave like a giant paramagnetic atom with fast response to applied magnetic fields with negligible residual magnetism and coercivity once the applied magnetics are removed (Fig. **1b** and **c**) [7].

There are several fields that robustly applied superparamagnetic properties into their mechanism application. For medical applications, magnetite (Fe_3O_4) and maghemite (γ-Fe_2O_3) are preferable and known as the highly recommended biomaterial due to their suitability for *in vivo* applications [8]. Integration of magnetic Fe_3O_4 nanoparticles into the microfluidic chip system, could cause a steering effect to the composite that guides the aggregated nanoparticles to the desired outlet microchannel. Thus making drug delivery process more manageable and efficient [9]. Madrakian [10] also reported that modification of the targeted drug (adsorbent) surface with Fe_2O_3, oxymetholone from urine sample can be constructed by applying the external magnetic field. The reusability was tested for five consecutive separations/desorption cycles under optimized conditions, which is cost-efficient with low detention limits and good relative standard deviation.

Another application is the ink-jet printed Superparamagnetic polymer composite (SPMPC) technology which made self-assembly possible by controlling and manipulating the magnetite-SU-8 anisotropy nanohemispheres to perform complex programmed fabrication [11]. Wireless application of SPMPC was performed along with external magnetic fields hence simplified the process in manufacturing components for microelectromechanical systems [12, 13].

In water treatment, photocatalysis is widely applied as a pollutant removal method. Photocatalysis is a process that utilized light as an activator to speed up the chemical reac-

*Address correspondence to this author at the Advanced Membrane Technology Research Center, Faculty of Chemical and Energy Engineering, Universiti Teknologi, 81310, Johor Bahru, Malaysia; Tel: +6 07 553 5352; E-mail: juhana@petroleum.utm.my

1876-4037/20 $65.00+.00

tion by engaging photo sensitive catalysts (photocatalysts). Photocatalysts need to be an inert solid that can promote reaction under the presence of light and inconsumable in the overall reaction. Generally, these reactions is to produce hydrogen peroxide (H_2O_2), protonated superoxide radicals (HOO•) and hydroxyl ions (•OH) by breaking down water compound under light radiation [14]. A good photocatalyst needs to be a light activator, possesses high redox potential, is biologically and chemically inert, is widely accessible and environmentally friendly [15].

In photocatalysis, performing the collection of IO nanoparticles is less complicated due to the structure form of photocatalysts that exists in powder form. The separation process between particles is practically easy once external magnetic field is applied. Mobtaker [16] was able to separate magnetite composite from the waste solution by applying the principle of magnet separation after the execution of methyl orange degradation test. Similar separation processes were also applied by developing ternary nanocomposite of graphene-TiO_2-Fe_3O_4 photocatalyst for organic dye degradation. Under UV radiation, graphene suppressed the TiO_2 charge carrier from fast recombination and enhanced the photodegradation of Rhodamine B dye. With the use of Fe_3O_4 as the magnetic separation unit, it allows the recollection of photocatalysts to take place [17]. The saturation magnetization value of magnetic samples can be tested by using the Vibrating Sample Magnetometer (VSM). Figure (**1c**) shows the magnetization curve for both γ-Fe_2O_3 and γ-Fe_2O_3/TiO_2 nanocomposite. The magnetization of the samples reached saturation values when external magnetic field increased to 10 000 Oe. The saturation magnetization was found to be 60.85 emu/g and 54.66 emu/g respectively. The small decrease was due to the surface modification but unavailing to its initial desired application [10, 18]. Magnetic photocatalyst shows promising properties that are easily separable and recoverable from treated water that can be engineered to meet other applications.

2. IRON OXIDE PHOTOCATALYSIS/ADSORPTION OPERATIVE PARAMETER

Several years, IO particles have shown impressive characteristic as good pollutant degradation material. The degradation process can be executed by using either UV or/and visible light radiation. The application is flexible since it can be excited with various light source radiation. For instance, adsorption process could occur either with the presence of light or in darkness. Moreover, IO absorbs light up to 600 nm, collecting up to 40% - 45% of the solar spectrum energy and mostly stable in aqueous solution [19-21].

Ling [6] had suggested pathways for photodegradation and adsorption mechanism of organic pollutant using iron oxide and illustrated the importance of free radical generations in photocatalysis (Fig. **2a**) including adsorption processes (Fig. **2b**). However, to grasp its optimum potential, researchers and scholars meticulously studied their behaviour under various parameters; pH value, physical properties, catalyst loading and reaction time.

2.1. Effect of pH Solution

The pH of the working solution changes the ion particles concentration at the surface of a ferric oxide photocatalyst and shifts the potential of some redox reactions [22]. Not only it changes the surface properties of α-Fe_2O_3 but also the dissociation of dye molecules and the formation of the hydroxyl radical [23]. In previous work, Zhu [24] studied the effects of pH solution on Methylene Blue (MB) dye degradation by adjusting the pH value on a magnetic stirrer. The minimum Methylene Blue (MB) dye concentration was obtained at pH 2. It is suggested that due to the acidic medium, the movement of the light-generated electron to hematite surface become easier. Promoting •OH and $•O^{2-}$ production and contribute to MB photodegradation. Similar result was obtained using Fe_3O_4 as a photocatalyst to degrade neutral red dye. High degradation activity tend to occur in acidic solutions due to the high concentration of H^+ ions competing effectively with positive dye cations [25].

Dyes have the tendency to decompose in acidic to neutral pH solution [26, 27], but Malachite Green (MG) dye shows in the favour of degrading under alkaline solution by hematite photocatalyst. According to Pawar and Khajone [28], as the pH value of a solution increases, the concentration of MG decreases. At the highest pH level of MG degradation rate (pH 10) indicated that the •OH is high at α-Fe_2O_3 surface which increases the coulombic attraction of cation dyes with negative charged catalyst surface. The diagram below shows the dye degradation in different pH values by using α-Fe_2O_3 photocatalyst.

The interpretation of pH effects on the efficiency of the photodegradation process is a very intricate task, because of its multiple roles. First, it is related to the acid base property of the metal oxide surface and can be explained on the basis of zero-point charge. The adsorption of water molecules at

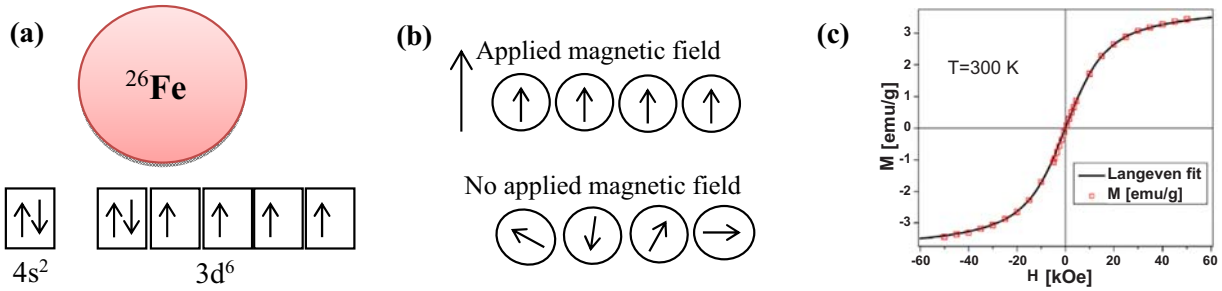

Fig. (1). Superparamagnetism iron oxide (**a**) molecular configuration, (**b**) superparamagnetic fast responds with and without magnet, and (**c**) VSM curve on superparamagnetic iron oxide [29]. (*A higher resolution / colour version of this figure is available in the electronic copy of the article*).

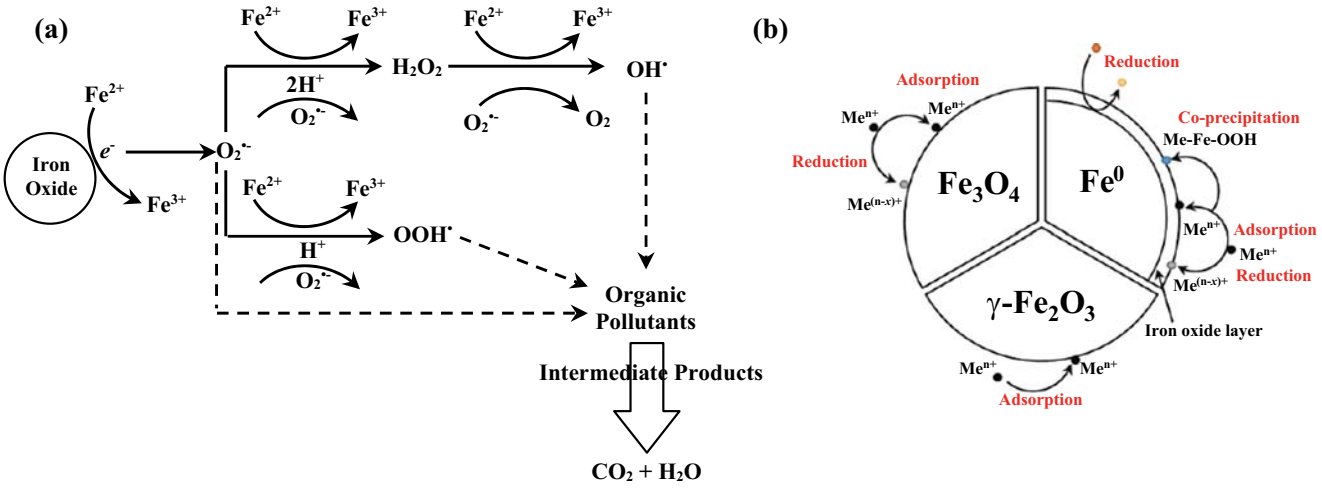

Fig. (2). (**a**) Photodegradation mechanism pathway for organic pollutants and (**b**) absorption process for iron oxide. (*A higher resolution / colour version of this figure is available in the electronic copy of the article*).

surficial metal sites is followed by the dissociation of OH^- charge groups, leading to coverage with chemically equivalent metal hydroxyl groups (M-OH) [30]. In order to create these 'working' condition, water sample needs to adjust to suitable pH value by adding strong acid / alkaline solution. Under highly acidic condition, IO are vulnerable to corrosion formation [31]. While by adding strong alkaline media, IO shows decreasing magnetization properties [32]. Hence, modification needs to be done to protect IO from further oxidation and magnetize loss.

2.2. Effect Morphological Structure of Iron Oxide Particle

2.2.1. Size

The effect of particle size can be observed proportionally through its surface area. Generally, the smaller the particle size leads to larger surface area and higher expected activity. This can be explained in term of an increase in the number of active sites per square meter, as well as greater adsorbability of the pollutant on the catalyst surface [33]. By heating and sonication aid, the hematite particle's surface became smoother and reduced in size. The modification had increased the photodegradation rate over ionic dye decomposition [22]. Minimizing the particle size using the synthesizing method [34], modifying calcination temperature [35], calcination duration, and pH value [36, 37]. In addition, adjustments in particle sizing could strongly influence the magnetism and electronic properties of the photocatalyst.

The DLVO theory was applied in a study to identify the aggregation of larger colloids and stability of α-Fe_2O_3 nanoparticles. The author had investigated the effects of particle size on nanoparticle agglomeration and stability under normal pH and ionic strength conditions. The DLVO prediction showed that the higher the ionic strength the higher the aggregation of the particles. This is caused by the attractive van der Waals forces that dominate over repulsive forces. The study also indicated that the effects of ionic strength on particle agglomeration increases with the decrease of particle size. As the particles size decreases, there is greater opportunity for the atoms to exist on the catalyst surface hence enhancing the density of active sites. However, the ferromagnetic properties of IO will be resulted in agglomeration hence decrease the active surface area.

To reduce the agglomeration formation, Baalousha [38] reported that the IO nanoparticles aggregate in diffusion limited aggregation mode where less than pH 2 will leads to formation of smaller aggregations (<50 nm) and as the pH increase, the repulsive forces between nanoparticles decrease causing particles to stick together. A comparative study was done between microstructures, nanostructures and micro/nanostructured α-Fe_2O_3 spheres (MNFs) to investigate their photocatalytic activity. First order kinetic shows MNFs react twice as fast as nanosized α-Fe_2O_3 spheres and 12 times faster than microsized α-Fe_2O_3 spheres for Rhodamine 6G (R6G) pollutant removal. The mixed structure of α-Fe_2O_3 works optimally in pH 6.5 solution, it is also able to control slow-release of OH radicals due to the complex porosity structure [39] and enhance the degradation efficiency. The superstructure of MNFs makes it reusable for several times without any decline in its photocatalytic ability [40].

Khedr [34] also proved that size does matter in photocatalytic activity even in the nano scales. The adsorption of Congo red dye using Fe_2O_3 nanoparticles and crystal size of 35 nm revealed to be the most efficient under tungsten bulb radiation and in the dark compared to 100 nm and 150 nm Fe_2O_3 nano-crystal. According to the decomposition rate results that obeyed the pseudo first-order kinetic reaction, an obvious decrease of degradation reaction was shown when using higher crystal size Fe_2O_3 where as it took less than 200 mins for 35 nm sized Fe_2O_3 to fully degrade Congo red under light irradiation and in the dark. It was also shown that the reaction rate constant for 35 nm Fe_2O_3 is 12 times greater than 100 nm and 5.5 times higher than 150 nm Fe_2O_3 under light radiation.

2.2.2. Shapes

Various shapes and morphologies of IO nanomaterial are experimentally available, each one with their own unique characteristic and application purposes had summarized the advantages of each dimensional shape of iron oxide; zero-dimensional (0D) shape usually possess strong quantum confinement effects and cause high recombination rate of generated charge carriers [6]. One-dimensional (1D) nanocrystals

with increasing ratio of length to diameter could restrict electron flow in the radial direction and instead guide the movement of electrons through the axial direction. It had been reported that aligned α-Fe_2O_3 nanotubes were able to achieve enhancement of surface area without an increase of the geometric area and reduce the scattering of free electrons, thereby, enhancing the electrons mobility. As for 2D nanostructures, they tend to provide larger reactive sites for surface reactions to occur and display fascinating charge barrier properties owing to its large surface area. Meanwhile, 3D structures provide high surface area and pore channels that allow higher mass transfer rates of the reactants and products (Table **1**).

The study on the effects of different dimensions of nanohematite was conducted by observing MB degradation rate. By adjusting duration and calcination temperature of the fabrication process, Chen and Lin [20] managed to synthesize nanoparticles (0D), nanorods (1D) and nanotubes (1D). Nanoparticles were found to gain the highest photocatalytic ability due to its large specific surface area (27.8 m^2/g) followed by nanotubes (25.5 m^2/g) and nanorods (20.8 m^2/g) and the results have proven to influence the degrading rate of MB dye at 400 min^{-1}, 450 min^{-1} and 550 min^{-1} respectively. Another study was also done on dimensional dependence on RhB degradation. Between the three different architecture structures of nano-hematites, nanorods illustrated the fastest decomposition of RhB dyes under visible light radiation. The protonic efficiency ξ of nanorods shows 0.012 %, compared to nanocubes (0.0083 %) and nanoplates (0.0072 %) [41].

2.2.3. Porosity

Porous catalyst offers high surface area [42] and exposes more active sites for redox reaction to occur. Cha [43] had synthesized porous α-Fe_2O_3 nanorods by the facile solution-phase approach under various heat treatments in air. They monitor grain size and pore diameter for 3 different reaction conditions of α-Fe_2O_3 nanorod and indicated that the smaller the grain size, the larger the specific surface area. There were two stages in light adsorption for MO degradation. First, spontaneous MO adsorption within 10 minutes (C/C_0= 0.38) followed by the second with a steady adsorption of MO from 10 to 60 minutes (C/C_0= 0.3). The porous nanorod removal capacity was calculated to be 34.5 mg/g and the MO removal was due to electrostatic attraction between catalyst surface and MO molecules.

Ahmmad [44] successfully used EGCG (Epigallocatechin gallate) and GCG (gallocatechin gallate) as surfactants to synthesize porous α-Fe_2O_3 nanoparticles by hydrothermal and biosynthesis techniques. The nature of both organic surfactants might be decomposition at high heat treatments and been washed with water and leaving pore in particles. The porous nanoparticles demonstrated surface area 4 times larger compared to commercialize α-Fe_2O_3 nanoparticles and double OH radicals yield under visible light radiation. With the micro- and macro-porous formed which resulted in larger active area, however, the high heat treatment will cause the porous to collapse and changed its shape.

2.3. Catalyst Loading

Catalyst loading parameter shows an interesting observation in determining the optimum weight of IO for the total efficiency of degradation rate. Generally, the removal rate of contaminant is linear to catalyst loading. However, it was observed that at a certain threshold (optimum loading), the reaction rate significantly and become independent of the catalyst concentration [45].

Liu [46] reported that the photodegradation efficiency of MB is directly proportional to electrospun α-Fe_2O_3 nanofiber loading from 20 – 50 mg/L. However, further increment up to 100 mg/L, shows a negative impact on the degradation rate. A similar observation was by Dang [47] that indicated the decolorization of reactive brilliant blue X-BR, that reaches the same saturated value at 0.1 g/L α-Fe_2O_3. As the loading increase to a certain level, the volume of catalyst will prevent light penetration [48] and increases the opacity of the suspension causing light to scatter which contribute to shielding effect.

Compared to dye degradation, removing metal ions in water needs more than 10 times the amount of IO catalyst; Cadmium (Cd^{2+},1 g/L) [49] and Uranium (U^{4+}, 2.5 g/L) [50]. According to the formation of As-Fe and As-O bond are monodentate and bidentate corner sharing complexes with Fe^{3+} crystalline. The 'bi' Lewis based ligand has the ability to 'grab' metal ions and formed Van der Waals interaction with each other on the IO surface [51]. The optimum catalyst dosage is found to be dependent on the initial concentration of adsorbate [52]. However it has the tendency towards agglomeration (particle-particle interaction) also increases at high solid formation, resulting in a reduction in catalyst surface area available for light absorption hence bringing little stimulation to the catalyst reaction [53].

2.4. Reaction Time

According to Langmuir, kinetics of the sorption process is related to the surface chemistry between the active sites (contact area) and the pollutant. Shirivastava [54] has synthesized Fe_3O_4 nano-adsorbent to observe its kinetic adsorption behavior for Zn^{2+} removal. By implementing both isotherm Langmuir and Freundlich kinetic model, the result shows R^2 = 0.99 from Langmuir pseudo-second-order. Fast adsorption reaction happened at the first 55 minutes and react slowly at a lower rate as it reached its equilibrium state after 2.5 hours of contact. Similar observation in degrading of reactive black 5 (RB5) dye has been studied where rapid adsorption occurred within an hour time with constant rate k_2 value of 0.001 L mg^{-1} min^{-1} [55]. Iram [25] suggested that the adsorption mechanism is highly dependent on the adsorbent (IO particles) and adsorbate (dyes, metal ions *etc*), which leads to surface exchange reaction. Electron-hole activation causing dye molecule to disintegrate hence explain the chemisorption phenomena of limiting step of pseudo-second-order to take place.

A further study on kinetic rate, Yoon [56] has excellently explained that the mechanism involves in pseudo-second-order adsorption process, where both physisorption and chemisorption does happen. He analyzed the binding energy and charge calculation for Oxygen (O, 1*s*) and Ferric (Fe, 2*p*) from X-ray Photoelectron Spectroscopy (XPS). The result shows only physical adsorption of phenol occurred on the surface of uncoated IO, while chemisorption (electron accepting) involved in methacrylic acid (MAA) coated IO.

Table 1. Different dimension and shape of iron oxide.

Dimension	Shape	Characteristic of the Obtained Product	Method	Specific Surface Area (m^2/g)	Degradation Rate	Adsorption Kinetic Model	Pollutant	Refs.
0D	Particles	The α-Fe_2O_3 particles present as granules with irregular spherical shaped particles with an average size between 19 – 37 nm.	Chemical precipitation	N/A	As the calcination temperature increases, the particles size also increases. This leads to a decline in specific surface area and causing decrement in photocatalytic activity.	Pseudo first-order	MB	[57]
	Cubes	Uniform distribution of microcubes with average edge size of 1535 nm, relatively rough surface texture	Hydrothermal	7.6 – 30.5 (varies depends on synthesis temperature)	MB was fully degraded within 12.5 minutes at 0.641 min-1 reaction rate. While both RhB and RB5 were degraded by 97% within 25 minutes and 40 minutes respectively.	Pseudo first-order	RB5, MB and RhB	[22]
1D	Rods	Smooth nanorod shaped with a diameter of 48 – 83 nm, length of 340 – 850 nm and porous with a diameter of 2 – 8 nm were formed.	Hydrothermal	27.28 – 96.73	Electrostatic attraction between MO and Fe_2O_3 nanorod enhanced the photodegradation where the removal capacity of the catalyst is 34.5 mg/g.	N/A	MO	[43]
	Tubes	Well-aligned uniform nanotubes Fe_2O_3 formed with oval and circular shaped on the top open surface, with an average diameter of 50 – 70 nm, and ~ 4 μm of length.	Electrochemical anodization	N/A	Sonicated clean nanotube Fe_2O_3 surface illustrates higher degradation rate compared to untreated nanotube hematite under visible light radiation.	N/A	MB	[58]
	Wires	Mesoporous needle-like shaped formed on the surface with an average diameter size of 30 – 35 nm, and a length of ~550 nm.	Hydrothermal	α-Fe_2O_3: 82 Fe_3O_4: 55.2	The active side of α-Fe_2O_3 wascreated by adding ZnO to the photocatalyst. MB and RhB show higher degradation rate compared to MO. The recovery rate shown to be 91 % retention up to 4 cycles.	Pseudo first-order	MB, RhB, MO	[59]
2D	Disks	Nanodisks formed with relatively rough surface with an average diameter of 100 nm and thickness of ~60 nm	Hydrothermal	15.19 – 174.6	The main absorption peak of MB at 664 nm shows a drastic decline in the first 10 minutes and continues to decrease over time.	Pseudo first-order	MB	[60]

(Table 1) contd….

Dimension	Shape	Characteristic of the Obtained Product	Method	Specific Surface Area (m^2/g)	Degradation Rate	Adsorption Kinetic Model	Pollutant	Refs.
	Platelets	Random oriented and uniform nanoplates with length, width and thickness of 300, 100 and 30 nm respectively formed.	Hydrothermal	69	Anisotropic growth of nanorod into nanoplatelets with surface area of 69 m^2/g had successfully degrading MB by 47.62% within 4.5 hours under solar light radiation.	N/A	MB	[61]
	Sheets	A formation that attributed from nanowire over longer heating period and higher temperature heat treatment, with less than 20 nm thick.	Thermal oxidation	70.866	Arsenic (As) and chromium (Cr) adsorption were conducted in pH 3 solution for 60 mins. 50 % As adsorption and a complete degradation of Cr were obtained after 10 minutes contact time.	N/A	Arsenic, Chromium ions	[62]
3D	Dendrites	Micropines structure with an average diameter of 4 – 6 µm, and branch truck range from 50 nm to 1.5 µm.	Reactable ionic liquid	N/A	90 % of MB was degraded within 150 minutes contact time. Where the absorption peak (664 nm) of MB shows gradual decrease leads to decolorize of blue dye.	N/A	MB	[63]
	Flowers	A uniform flower-like microstructure with an average diameter of 3-5 µm. Each 'flower' consists of aligned nanorods with an average diameter of 100 ± 10 nm and an average length of 900 ± 100 nm growing from its center.	Hydrothermal	N/A	63 % of RhB were decomposed within 60 minutes under UV light. Adding another 50 mg had shortened the degradation time by half.	N/A	RhB	[64]
	Urchins	An urchin shaped formation that made of highly dense nanoneedles assembled at one center point. The nanoneedles with an average length of 110 ± 30 nm, and a full urchin size of 2 ± 0.5 µm in diameter.	Hydrothermal	~76.703	Under visible light radiation, α-Fe_2O_3 nanourchin was able to photodegrade Cr by 98 %, followed by ER (84%) and MB (80%).	Pseudo first-order	CR, ER, MB	[65]
	Spheres	A connected hollow nanoparticle that forms nanospheres with an average diameter of 200 – 300 nm.	Hydrothermal	0.0756	The maximum absorption was in the pH range of 5.5 – 6 with 105 mg of dye for 0.05 g Fe_3O_4 nanospheres.	Pseudo second-order	Natural Red	[25]

*RhB: Rhodamine B; RB 5: Black 5; MB: Methylene Blue; MO: Methyl Orange; CR: Congo Red; ER: Eosin Red.

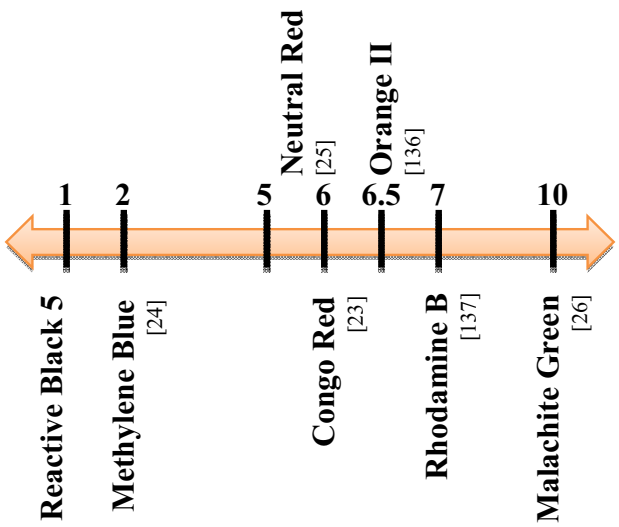

Fig. (3). Organic dyes degradation by ferric oxide at different pH value.

Maji *et al*. [66] observed the photocatalytic activity of mesoporous α-Fe_2O_3 nanoparticles under 200 W tungsten light radiation. From the linear extrapolation of reactive blue photodegradation rate expressed by ln (C_0/C_t) = kt, the constant pseudo-first-order k_1 rate is 0.00265 and 0.00157 min^{-1}. Different with adsorption, photodegradation mechanism contain several steps [67] ; 1) photocatalyst activation 2) electron-hole generation 3) transfer of charge carrier from valence to conduction band 4) recombination of charge carrier during the photodegradation process.

A significant colour change shown under designated period due to visibility of dye degradation processes (Fig. **3**). Huang [60] had monitored the MB colour change for 60 minutes under visible light illumination [51]. A noticeable decolorization occurs between first 10 to 20 minutes time interval where the adsorption intensity decreased drastically and turn to clear solution as the exposure time reach to an hour. With prolong light radiation time, the initial MB solution underwent a colour changing process of blue, light blue and eventually colourless solution [24], which illustrates a complete degradation of the chromophoric group. The Fig. (**4**) shows the possible mechanism for Methylene Blue (MB) dye photo-decolorization. The activation of electron-hole on photocatalyst surface yielded OH group upon in contact with water. The OH radicals will attack the C-S^+=C functional group in MB, by initiating the degradation process by electrophilic attack on free doublet of heteroatoms S. The path from C-S^+=C to C-(S=)-C requires the conservation of the double bond conjugation, which induces the opening of the central aromatic ring containing both heteroatoms, S and N. The origin of H atoms necessary to C–H and N–H bond formation can be proposed from the proton reduction by photogenerated [68].

3. MODIFICATION OF IRON OXIDE FOR IMPROVED PHOTOCATALYTIC ACTIVITIES

As mentioned in the previous section, iron oxide had proven to be a reliable and efficient photocatalyst. Despite their advantageous features, its hydrophobic surface and high surface energy tend to agglomerate and form large clumps, which increases the particle size [69-71]. High recombination rate of electrons and holes led to poor photocatalytic activity which resulted in photocorrosion and limiting its full potential [4, 9, 21]. Therefore, researchers and scholars had suggested a few methods to overcome these limitations.

3.1. Photodissolution Prevention

Photodissolution is a phenomenon of photocorrosion under an electron transfer reaction *via* localized sites of the semiconductor [72]. The iron oxide photodissolution process take place in the eq. 1; (a) interface of IO/water, where the ferrous ions greatly enhance the rate of (b) incorporation of further iron (Fe(III) to the aquatic medium which (c) leads to Fe(II) formation) [73]. Evidence had shown exhibition of light adsorption due to electron-hole pairs in the results from electron traps occurrences which then produces dissolution sites.

There are few suggestions made to suppress photodissolution from happening. The first approach is to couple it with other semiconductors to form heterojunction composites. Direct contact between the molecules interrupt the occurrence the electrons-holes recombination due to continued charge carrier transfer within the coupled photocatalysts. Example of this type of heterojunction structures includes the composite of TiO_2/α-Fe_2O_3 [74-76], ZnO/α-Fe_2O_3 [77-79], WO_3/Fe_3O_4 [80] and SnO_2/Fe_3O_4 [81]. These studies illustrated that small band gap energy of iron oxide was able to capture the visible light spectra to excite electrons to rise from valence band to conduction band and being to its neighbour semiconductor. In this context, iron oxide acts as electron initiator since it is more cathodic compared to its coupled material [6].

Another precautionary step is by adding an inert layer or shell to form indirect contact of heterojunction photocatalysts. Silica (SiO_2) is usually applied in this set-up [82, 83]. In this case, iron oxide only acts as retrieving mechanism in photocatalysis process. The addition of SiO_2 is to prevent any direct interaction between the semiconductors that leads to electron-hole transfer, which result in photodissolution.

3.2. Improving Hydrophilicity

Iron oxide is an ionic bonding molecule that consists of two ferric ions and three oxygen ions. It is hydrophobic by nature, and the hydrophobic interaction between the molecules cause agglomeration. Several previous works show a different material selection based on functional groups for hydrophilicity alteration purpose as presented in (Fig. **4c**). Studies indicated that graphene, Graphene Oxide (GO), reduced Graphene Oxide (rGO), Silicon Oxide (SiO_2) and reactive carbon do contribute to enhanced hydrophilic properties (Table **2**). According to Stobinski [84] there are four different functional group peaks that can be found in GO and rGO which contribute to surface modifications. The XPS results show high content of functional oxygen contents in both samples; hydroxyl (-OH), epoxy (-O-), carbonyl (-C=O), and carboxyl (-OOH). In rGO, the C/O ratio seems to be higher than GO, but decreased twice as much in terms of C sp^3 hybridization composition due to additional water content that leads to layer delamination formation. The XPS results show similar main functional groups of activated carbon with the

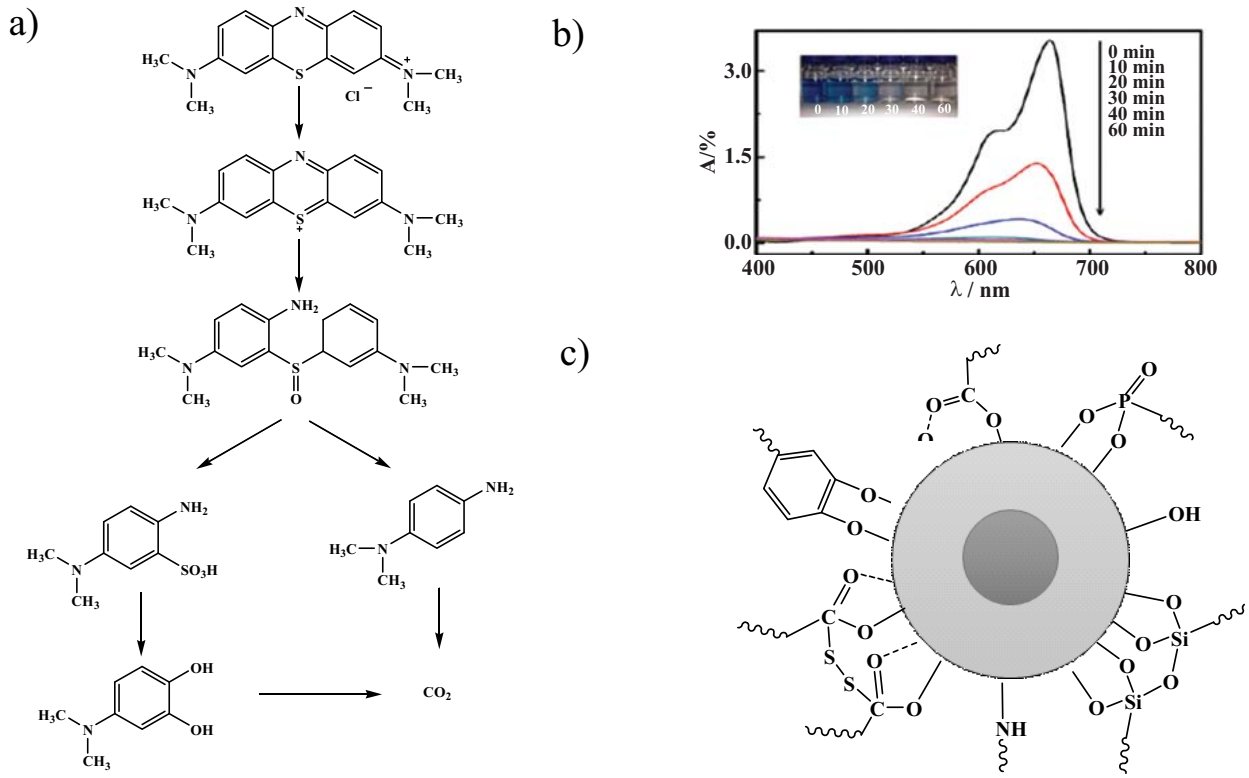

Fig. (4). Photodegradation of MB (**a**) suggested mechanism breakdown pathway, (**b**) visual observation on decolorization over 60 mins duration, and (**c**) possible ligands form between iron oxide and other functional groups. (*A higher resolution / colour version of this figure is available in the electronic copy of the article*).

Table 2. Summary of functionalization approaches on iron oxide.

Type	Material	Functional Group/ionic Charge	Remarks	Refs.
Graphene based	Graphene	Hydroxyl, -OH Epoxy, -O- Carbonyl, -C=O Carboxyl, -COOH	Enhanced distribution, Binding capability, Biocompatibility.	[85, 86]
	GO	Hydroxyl, -OH Epoxy, -O- Carbonyl, -C=O Carboxyl, -COOH	The surface functionality greatly weakens the platelet-platelet interactions, owing to its hydrophilic properties.	[87-89]
	rGO	Hydroxyl, -OH Epoxy, -O- Carbonyl, -C=O Carboxyl, -COOH	High adsorption rate due to its high specific surface area.	[84, 90, 91]
	Activated carbon	Carboxyl, -COOH Epoxy, -O- Hydroxyl, -OH Carbonyl, -C=O	Ferric ions introduced more acidic functional groups to the carbon surface hence provided more adsorption side for negative charge ions to be removed.	[92-94]
Organic	Chitosan	Carbonyl, -C=O Epoxy, -O- Hydroxyl, -OH Amine, -NH_2	Trough alkaline solution, biocatalytic protein by protonate.	[95, 96]

(Table 2) contd….

Type	Material	Functional Group/ionic Charge	Remarks	Refs.
	Gelatine	Carbonyl, -C=O, Hydroxyl, -OH Amine, $-NH_2$	Gelatine has many metal coordinate site that will form polymer-metal complex.	[98, 99]
Bipolar Surfactant	Tetramethylammonium Hydroxide (TMAOH)	Hydroxyl, -OH Amine, $-NH_2$	Magnetite surface coated with $(CH_3)_4N^+$ cations after been treated with TMAOH.	[100]
	Tetramethylammonium 11-aminoundecanoate	Carbonyl, -C=O Amine, $-NH_2$	Resulting in biocompatibility properties and promising a bio-application.	[101]
Inorganic	TiO_2	Ti^{4+}, O^{2-}	The reduction of Ti^{4+} cation to Ti^{3+} cation state and oxidized O_2^- anions to evolved O_2 that leads to production of OH group hence increase the hydrophilicity.	[102-104]
	Montmorillonite clay	$(Na,Ca)_{0.33}(Al,Mg)_2$ $(Si_4O_{10})(OH)_2{\cdot}nH_2O$	High cation exchange capacity.	[105]

GO compound [92]. A projected mechanism of surface bonding between active carbon and ferric ions is shown in (Fig. **5a**). In relation to that, Liu [93] suggested that the Lewis base interaction between highly oxygen functionality compound with ferric ions was created, thus enhancing the hydrophilicity of the adsorbent was also discussed. The mechanism of fast deprotonation of TAC/Fe surface for Cr (IV) removal (Fig. **5b**).

Another approached by Anjaneyulu [90] is by adding another rGO layer supported MoO_3/Fe_2O_3 as a tertiary nanocomposite, in which each component plays a different role in MB removal. The hydrophilic properties of both MoO_3 and rGO have successfully improved the hydrophilicity of the tertiary nanocomposite. The addition of rGO into the heterogeneous MoO_3/Fe_2O_3 nanoparticles have enhanced the MB photodegradation yield. The rGO layer not only improve the hydrophilicity, it also provides more photocatalytic active sites. Even though adding another layer or component into binary composite will provide additional 'hand', the result may not be in favour, because the 'overcrowd' composition will lead to size increment, less active sites and leaching problem.

3.3. Improving Recombination Rate

As explained earlier, IO tends to face high recombination rates due to its short band gap energy. The responsibility of a photocatalyst is its capacity to undergo redox reaction once the enough energy is provided. The semiconductor must able to perform reduction of the proton at E_{NHE} (H^+/H_2) = 0.0 eV, and the oxidation of water at E_{NHE} (O_2/H_2O) = 1.23 eV simultaneously [4, 97]. More specifically, the redox potential of the donor species (OH groups) react with the valence band holes to yield hydroxyl radicals, •OH, at E_{NHE} (OH^-/•OH) = 2.5 eV. These three reactions ((H^+/H_2), (O_2/H_2O) and (OH^-/•OH)) are considered as the overall charge transfer activity that occurred continuously during photocatalysis process.

Referring to Fig. (**6**), magnetite possesses the shortest band gap (0.1 eV) while γ-Fe_2O_3 and α-Fe_2O_3 has similar band gap value of 2.3 eV and 2.2 eV respectively. They all can easily be activated under visible light, however for Fe_3O_4, due to its narrow band gap, it leads to faster recombination of electron-hole pairs compared to the other two which will decrease the photocatalytic activity. Under visible light radiation on both γ-Fe_2O_3 and α-Fe_2O_3 particles, the negative electrons valence band will further chemisorbed oxygen ($e^- + O_2 \rightarrow \bullet O_2^-$) and form $\bullet O_2^-$ radicals [70]. While accumulated holes in Fe_2O_3 valence band will react with OH^- to product hydroxyl group. The production of superoxide radicals ($\bullet O^{2-}$) undergo a transformation ($\bullet HO_2 + \bullet HO_2 \leftrightarrow H_2O_2 + O_2$) to yield active oxygen species such as •OH, $\bullet HO_2$ and H_2O_2 which will highly increase the degradation rate. Although the band gap of Fe_2O_3 suggests utilization of wider range of solar spectra, the application is limited by the VB position of Fe_2O_3 which is more positive in comparison to the H^+/H_2 electrode making it unsuitable for H_2 production the more negative position of VB of H_2 potential. The most suggested method is by doping IO with higher band gap semiconductor to form heterogeneous coupling. The added semiconductor could defect the IO surface hence provide electron "stopover" junction that will delay and supress the recombination for happening [106-108]. Chirita and Grozescu [4] suggested the implementation of charge carrier trapping approach into the system will delay and prolong the separated electron-hole recombination activity. To accommodate this theory, photodegradation rates play an important role in the indication the coupling semiconductor effectiveness. Sánchez [109] studied the effects of multilayers of TiO_2, Fe_2O_3 and TiO_2/Fe_2O_3 catalysts of MB organic dye. Under visible light radiation, the TiO_2/Fe_2O_3 layers removed MB faster than the TiO_2 and Fe_2O_3 layers. The results showed that there were two degradation phases occurring in the TiO_2/Fe_2O_3 for the duration of 600 minutes. The first 100 minutes, the catalyst performed as photodecomposition by TiO_2 catalyst [67, 110] and was replaced by Fe_2O_3 photocatalytic characteristics after 200 minutes of reaction. The combination of photocatalytic mechanisms indicates the OH radical groups present on the surface of Ti and Fe atoms that competes for MB compound adsorption [111]. Therefore, it is highly recommended that iron oxide collaborated with other materials to overcome and enhance the overall photocatalytic activity.

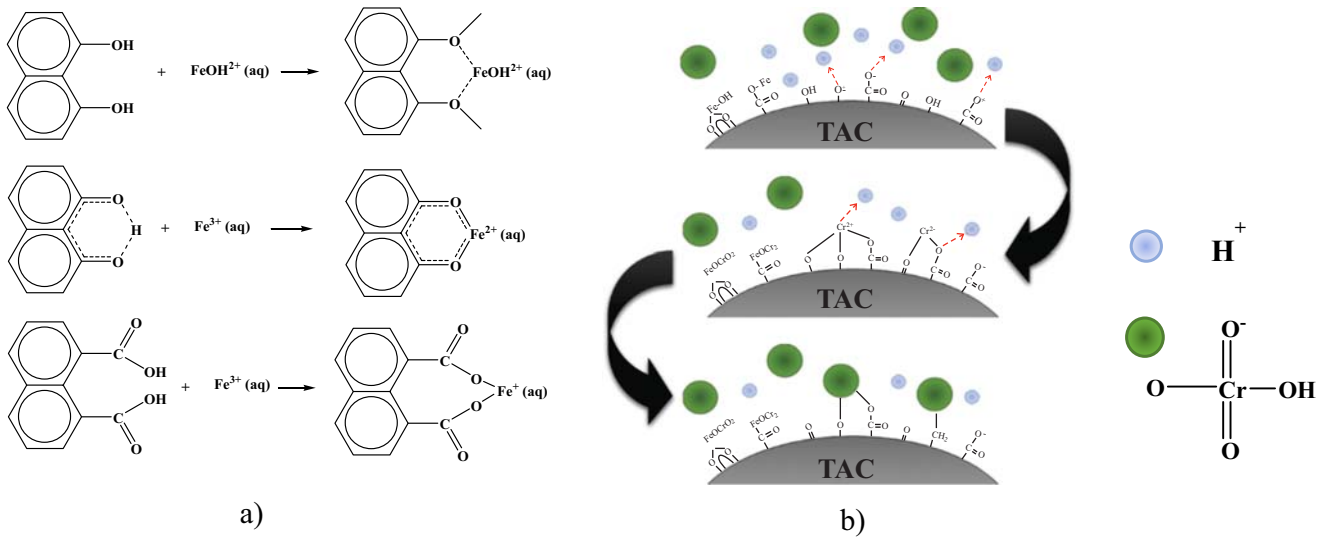

Fig. (5). (**a**) Surface chemical of difference functional group towards ferric ions, and (**b**) schematic process of Cr(IV) removal by TAC/Fe catalyst. (*A higher resolution / colour version of this figure is available in the electronic copy of the article*).

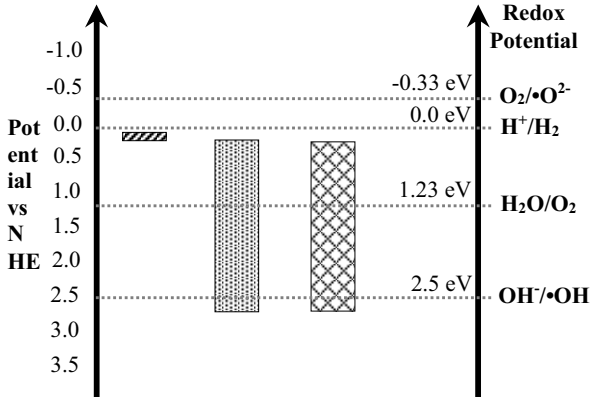

Fig. (6). Energy level diagram of Fe_3O_4, γ-Fe_2O_3 and α-Fe_2O_3.

Besides TiO_2, ZnO particles show a great coupling semiconductor candidate for the same application. Xie [112] formulated different α-Fe_2O_3 to ZnO loading ratio photocatalyst for pentachlorophenol degradation. Under UV-light radiation, because of the presence of α-Fe_2O_3 that able to extend the optical absorption edge of ZnO from UV light to visible light spectrum, the photodegradation of pentachlorophenol is almost completely decomposed with 1:5 molar ratio α-Fe_2O_3/ZnO within 4 hours. Another study has been conducted to improve the degradation time by adding g-C_3N_4 into the α-Fe_2O_3/ZnO. PL spectroscopy shows the decline peak at 463 nm of g-C_3N_4 pristine after α-Fe_2O_3 was decorated into g-C_3N_4/ZnO ternary nanocomposites. The result explained a slower in recombination rate of photoinduced charge that attributed to a successfully degradation of 99.34% of tartrazine within 35 min under visible light irradiation [113].

Kar [114] has synthesized two types of heterojunction photocatalysts Fe_2O_3/BOC1 and Fe_2O_3/BOC2 that exhibit efficient visible light driven Cr (IV) and MB dye photodegradation under continuous flow system. They reported that Fe_2O_3/BOC1 formation shows the highest pseudo-first-order rate constant (K_{app}) value of 0.014 min^{-1}, which demonstrates efficient Cr (IV) photoreduction and illustrates ~100% photodegradation of MB within 160 minutes. Others heterojunction coupling such as Fe_2O_3/Cu_2O [115], Fe_2O_3/Bentonite [116] and Fe_2O_3-CdS [117] are also designated to operate better under visible light radiation.

4. MECHANISM AND PERFORMANCE OF POLLUTANT REMOVAL BY ION OXIDE

In photocatalyst applications, the mostly studied area are limitations and decomposition of pollutants in the water treatment process. The ability to supervise these methods under visible light radiations and iron oxide modifications are beneficial to managements of global water. Wastewater from different sources has made water treatment processes complicated and limited. For example, in industrial wastewater, it is a norm to hazardous toxic metal waste if proper separation and treatment systems are not meticulously conducted.

The classification of targeted pollutants is indeed crucial to obtain efficient removal technique. In this paper, we focus on the removal of Natural Organic Matter (NOM), inorganic metal ions, and microbial pollutant will be comprehensively discussed.

4.1. Natural Organic Matters (NOM)

Natural Organic Matter (NOM) is considered a complex matrix comprising a heterogeneous mixture of organic compounds such as humic substance, polysaccharides, amino sugar, proteins, peptides, lipids, small hydrophilic acids, and others [118]. Conventional wastewater treatment technology does not eliminate these pollutants completely but disciple it to other phases [119], causing pungent smell, generating secondary toxic pollutant and bringing harmful surrounding to the ecosystem.

NOM that exist in water possess both hydrophilic and hydrophobic components. The hydrophobic part mainly consists of aromatic carbon, having phenolic structures and conjugate double bonds, while hydrophilic NOM is rich in a higher proportion of aliphatic carbon and nitrogenous compounds, such as carbohydrates and proteins, sugars and amino acids [118].

Disintegrating organic matter with aromatic carbon structures challenging task since it possesses stable and strong phenolic structures and C = C bond. Components such as estradiol, glucocorticoids, tannic acid, caffeic acid, eugenol, nonylphenol are present in domestic sewage through domestic and industrial wastes. These chemical have a tendency of undergoing transformation into other moieties, which severe health risk to humans, animals, and marine life [120, 121].

Oxygen in adsorbance surface functionalities can be essential for π – π interaction phenol adsorption/photocatalysis. In π – π bonding, oxygen atoms, reduce the π electron density and weaken the dispersion forces between the phenol and the surface functional group carbon [56]. Back in 1995, Pulgarin and Kiwi [122] studied the effects of α-Fe_2O_3 on aminophenol photodegradation. They observed the initial fast-induced ring dearomatization followed by slower disintegration of the aliphatic intermediate (Fig. **7**).

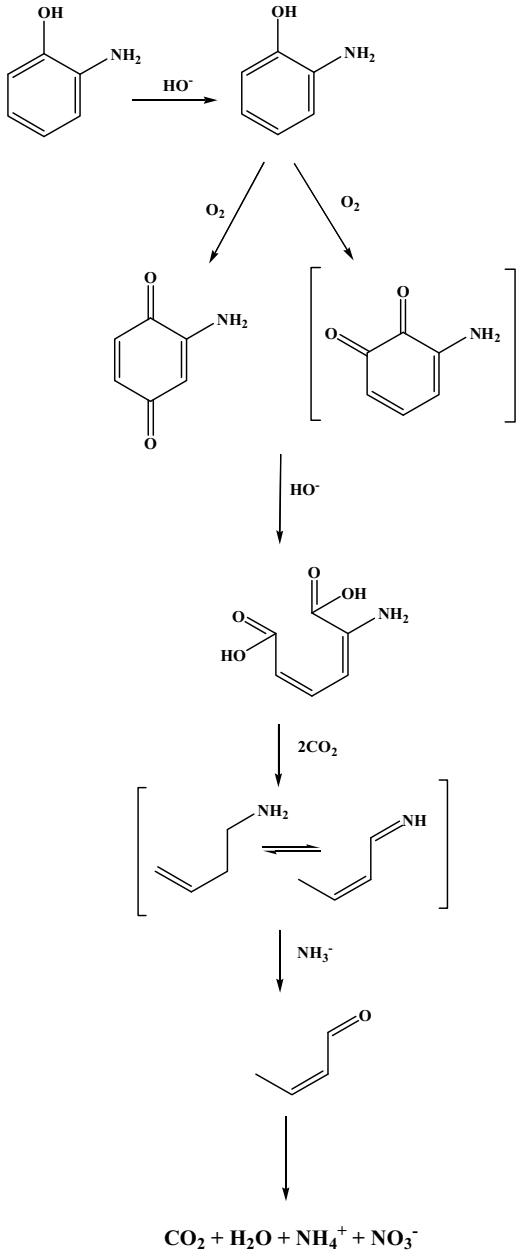

Fig. (7). Suggested pathway for 2-aminophenol.

In the presence of oxygen, redox reactions took place within Fe(III) surface and formed ligand-metal charge transfer processes, thus producing electron-hole that led to yield of OH^-. Due to the lack of photoproduced holes in converting OH- into OH radicals, they suggested that the photodegradation of 2-aminophenol is more due to surface complex rather than semiconductor assisted photodegradation.

Similar structures of 4-nitrophenol (4-NP) were monitored to study its mineralization degree mechanism by exposing it to TiO_2/α-Fe_2O_3-supported bentonite heterogeneous photocatalyst. Under UV light radiation, 78 % COD removal rate was recorded with increments of H_2O_2 generation by 224.59 μmol/L and 98 % 4-NP photodegradation. However, after 150 min of radiation, the H_2O_2 content decreases. It may be due to photodissociation reaction, and/or formation of Fe^{3+} and Fe^{2+} complex state by H_2O, which lead to photodegradation of 4-NP (Fig. **8**) [123].

4.2. Heavy Metal and Ions

Most industrial wastewater contain heavy and toxic metal ions, causing disruption to the environment and marine life. In general, heavy metal toxicity can cause chronic degenerative diseases, mental disorders, muscles and joints pain, gastrointestinal disorders, vision problems, chronic fatigue, and fungal infections [1]. In contradiction NOM degradation, heavy metal removal requires another set of mechanism to eliminate it from the water system. Most commonly found metal ions are Cd^{2+}, Cr^{3+}, Pb^{2+}, Zn^{2+}, and As^{3+}, where highly accessible adsorption site and high surface areas are favourable.

Arsenic is a very common toxic pollutant that is widely disposed in natural water. The United States Environmental Protection Agency (US EPA) have provided maximum arsenic contaminant level at 0.01 mg/L for drinking water in 2001. The quality water supply need to meet the new standards that was improved in 2006 [124]. Mayo [125] had observed that the magnetite particles vary in arsenic removal. Three different nanoparticle sizes (300 nm, 20 nm, and 12 nm) were prepared by the one-pot synthesis method and 12 nm Fe_3O_4 illustrated the photodissociation reaction, and/or formation of Fe^{3+} and Fe^{2+} complex state by H_2O. Arsenic shows two different ionic charges (As^{3+} and AsO_4^{3-}) in water. Using γ-Fe_2O_3/TiO_2 nanoparticles as adsorbent, Yu [126] has identified that arsenite (As^{3+}) adsorbed effectively under acidic solution. As the pH value increases (alkaline), removal of arsenate (AsO_4^{3-}) shows significant changes as well. (Table **3**) shows the iron oxide based photocatalyst/adsorbent for metal ion removal.

4.3. Organic Dyes

Organic dyes approach is frequently used in several studies as target pollutants. By observing the decolourization progress, it significantly justified the removal efficiency of the photocatalyst/adsorbent. Generally, organic dyes are soluble coloured substances that convey colour by selective adsorption light. The decolorization and photodegradation of dye be observed by the disintegration of chromophores molecules from covalent main chains. This is achieved by injecting OH groups from redox reaction of photocatalytic activity. For example, co-precipitated CuO/α-Fe_2O_3 powder

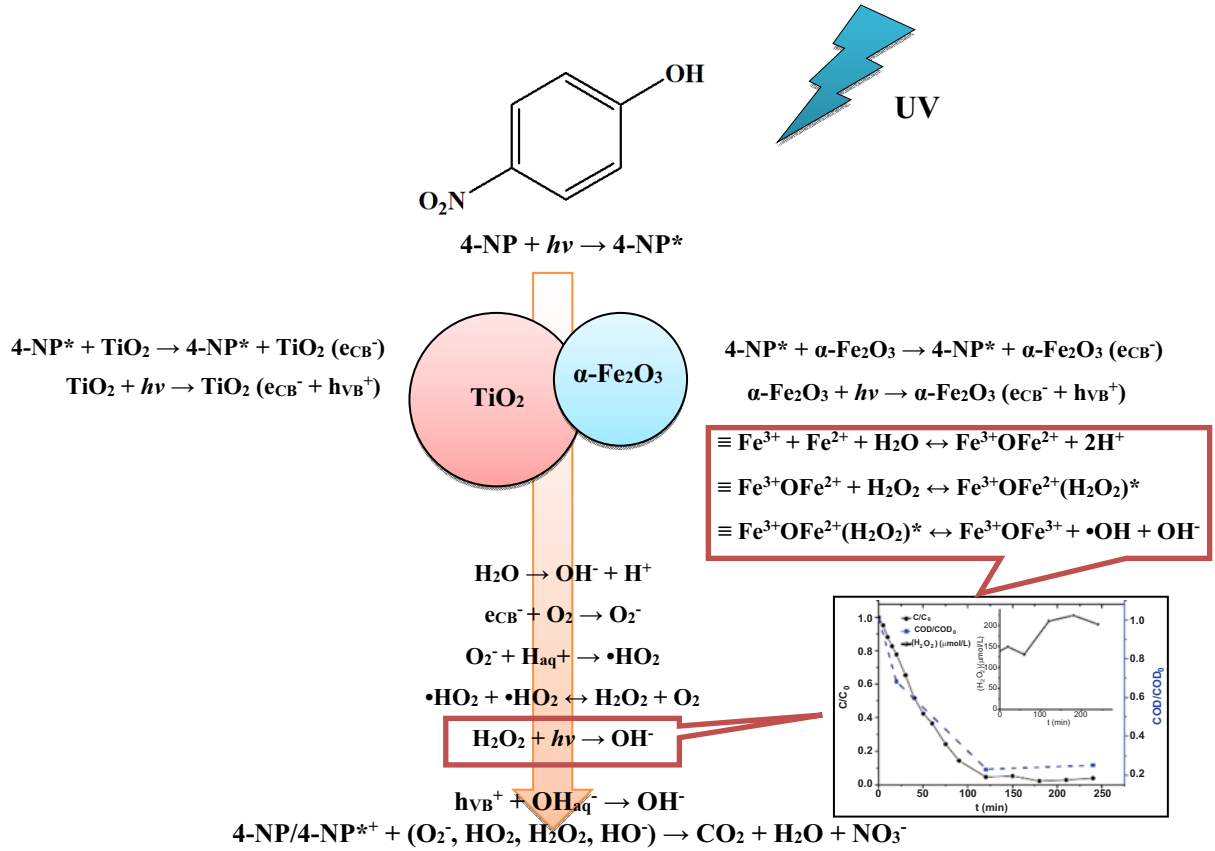

Fig. (8). 4-NP photodegradation process. (*A higher resolution / colour version of this figure is available in the electronic copy of the article*).

Table 3. Iron oxide based photocatalyst/adsorbent for metal ion removal.

Metal Ions	Absorbent/ Photocatalyst	Parameter	Key Finding	Refs.
Anion				
Chromium, Cr	3D-flowerlike iron oxide	Iron oxide type	• γ-Fe_2O_3 possessed the highest surface area 56 m^2/g, followed by α-Fe_2O_3 (40 m^2/g) and Fe_3O_4 (34 m^2/g). • α-Fe_2O_3 gain the highest Cr removal by 4.47 mg/g and Fe_3O_4 at 4.38 mg/g also γ-Fe_2O_3 is 3.86 mg/g.	[127]
	γ-Fe_2O_3 beads	pH solution, radiation duration	• Photo-reduction significant at lower pH value. • Under solar radiation, Cr (IV) completely reduced after 50 minutes.	[128]
	Fe_3O_4-montmorillonite	Synthesis method	99.8 % removal was shown at pH between 2-2.5, and gradually decrease as to higher pH value.	[105]
	Iron oxide-carbon nanotubes	Different type of iron oxide	The adsorption rate is higher than multiwall carbon nanotubes and activated nanotubes.	[129]
	Nanoporous Fe_2O_3	Synthesis method	Degrade 82.11% of Cr (IV) within 120 min under visible light radiation.	[130]
Arsenic, As	Fe_3O_4	Nanocrystalline size	12 nm magnetite removed 99.2% of As(III) and 98.4% of As(V).	[125]
	3D-flowerlike iron oxide	Iron oxide type	• γ-Fe_2O_3 possessed the highest surface area 56 m^2/g, followed by α-Fe_2O_3 (40 m^2/g) and Fe_3O_4 (34 m^2/g). • α-Fe_2O_3 gain the highest As removal by 5.31 mg/g and γ-Fe_2O_3 at 4.75 mg/g also Fe_3O_4 is 4.65 mg/g.	[127]
	γ-Fe_2O_3-TiO_2	pH	Acidic pH condition favours to As(V) adsorption while As(III) removal efficiently in alkaline solution.	[126]
	γ-Fe_2O_3-Zeolite (MNCZ)	Synthesis method	The optimum removal of 99.39% As at 2.5 pH with 20mg/L initial As concentration.	[131]

(Table 3) contd….

Metal Ions	Absorbent/ Photocatalyst	Parameter	Key Finding	Refs.
Cations				
Lead, Pb	Fe_2O_3-G-C_3N_4	Doping method	3 wt% Fe_2O_3 was the optimal doping ratio, and shows complete photodegradation of Pb ions under visible light within 60 mins.	[132]
	Fe_3O_4-SiO_2	pH, regeneration ability	Pb^{2+} reduced from 10 to 0.306 mg/L (97 %) within 10 mins of stirring. pH 6 shows its optimum removal rate.	[130]
Cadmium, Cd	Alumina-Fe_3O_4	pH, Temperature, adsorbent dose, contact time, initial Cd^{2+}	Magnetic alumina prone to remove Cd^{2+} at pH 6 within 240 min.	[49]
	Bentonite clay- Fe_3O_4	Effect of bentonite clay	The Cd^{2+} ions tend to replace Fe^{2+} and Ca^{2+} that resulting low adsorption efficiency.	[133]
Zinc, Zn	Fe_3O_4	pH, adsorbent dose, contact time, Zn initial concentration	• Reached equilibrium state after 2.5 hours of contact. • Optimum operation pH is at 5.5. • Removal efficiency reached its highest peak at 2.5 mg/L.	[54]
Copper, Cu	γ-Fe_2O_3-calcium alginate	pH, adsorbent dosage, Cu^{2+} initial concentration	The optimum pH is at 2, 2.0 mg/L adsorbent dosage for 250 mg/L Cu^{2+} concentration.	[134]
Mercury, Hg	Mixture of Fe_3O_4, γ-Fe_2O_3	Synthesis method	Mercury (Hg) removal > 85 %, using low concentration (< 10mg/L) of iron oxide nanoparticles solution.	[135]
	Fe_3O_4-SiO_2	pH, regeneration ability	Hg^{2+} reduced from 10 to 0.588 mg/L (94 %).	[130]
Radioactive				
Uranium, U	Fe_3O_4-SiO_2	pH, Absorbent dosage, shaking time, initial U concentration	The maximum U sorption was around 52 mg/g at 25 °C. pH 6 condition illustrated the highest removal rate (98 %).	[50]
	Fe_3O_4-TiO_2	pH, temperature, contact time	The maximum adsorption was at pH 6 with 118.8 mg U/g	[18]

successfully photodegraded methyl orange (MO) azo dye at its optimum condition (C_{CAT}= g/L, C_{MO}= 15mg/L, and pH= 6) under visible light radiation [136]. The azo chromophoric group that was presented in MO were detached from the main chain, and the chain breaking process continued until it reaches its maximum degradation rate at 88.47%. The same goes to other azo type dyes, methylene blue [82], reactive red [48] and reactive black-5 [55]. The reduced chromophoric group concentration may explain the decolorization process and emphasize the role of OH radicals in photodegradation activity. Fig. (**9**) shows the chromophoric group dyes and its dye compound.

4.4. Microbials

Exposing oneself to bacteria can result in serious illness and could cause death. Microbial such as bacteria, protozoa and viruses are highly concentrated in ground and open water [47]. Therefore, it is crucial and significant to develop effective, low cost, environmentally sustainable and friendly biocides. Magnetic-based photocatalysts have shown remarkable photocatalytic disinfection of bacteria and its magnetic separable ability that highly desired. Superparamagnetic separable Fe_3O_4-SnO_2 photocatalyst were prepared by hydrothermal and sonochemical methods. The two methods resulted an impressive photodegradation of *Escherichia coli* (*E. coli*) under visible light. However hydrothermal approach performed better than the sonochemical sample.

Hydrothermal method produces higher specific surface area which exhibits larger active sites for photocatalysis process [81]. Fluorescence spectroscopy has been used to observe *E. coli* bacteria cell inactive behaviour due to the membrane damage rate over time by Fe_2O_3/AgBr photocatalyst. The prolong cell damage has proven to be the further process of photo-generated h+ in the *E. coli* inactivation [137]. Ma [138] reported that by incorporating Fe_3O_4 with TiO_2 nanosheets (TNS) *via* the solvothermal method, it can photodegrade 87.2% of *E. coli* and 93.7% of *Staphylococcus aureus* (*S. aureus*) under visible light radiation. He also proposed that due to the excellent conductivity properties of Fe_3O_4, the Fe_3O_4-TNS composite can separate photoinduced charge carrier faster than TNS hence increase its photocatalytic activity. There were also two separate antibacterial mechanism involved in disintegrating *E. coli* and *S. aureus*. For Gram-negative *E. coli*, the cell body was easily distorted and ruptured by reactive species (•OH, H_2O_2 and $•O_2$). On the other hand, Gram-positive *S. aureus* shows no noticeable membrane destruction, and the cell surface was covered by massive Fe_3O_4-TNS, that suggests the restricted activity route and resulting in malfunction of the selective permeable barriers and the death of cells.

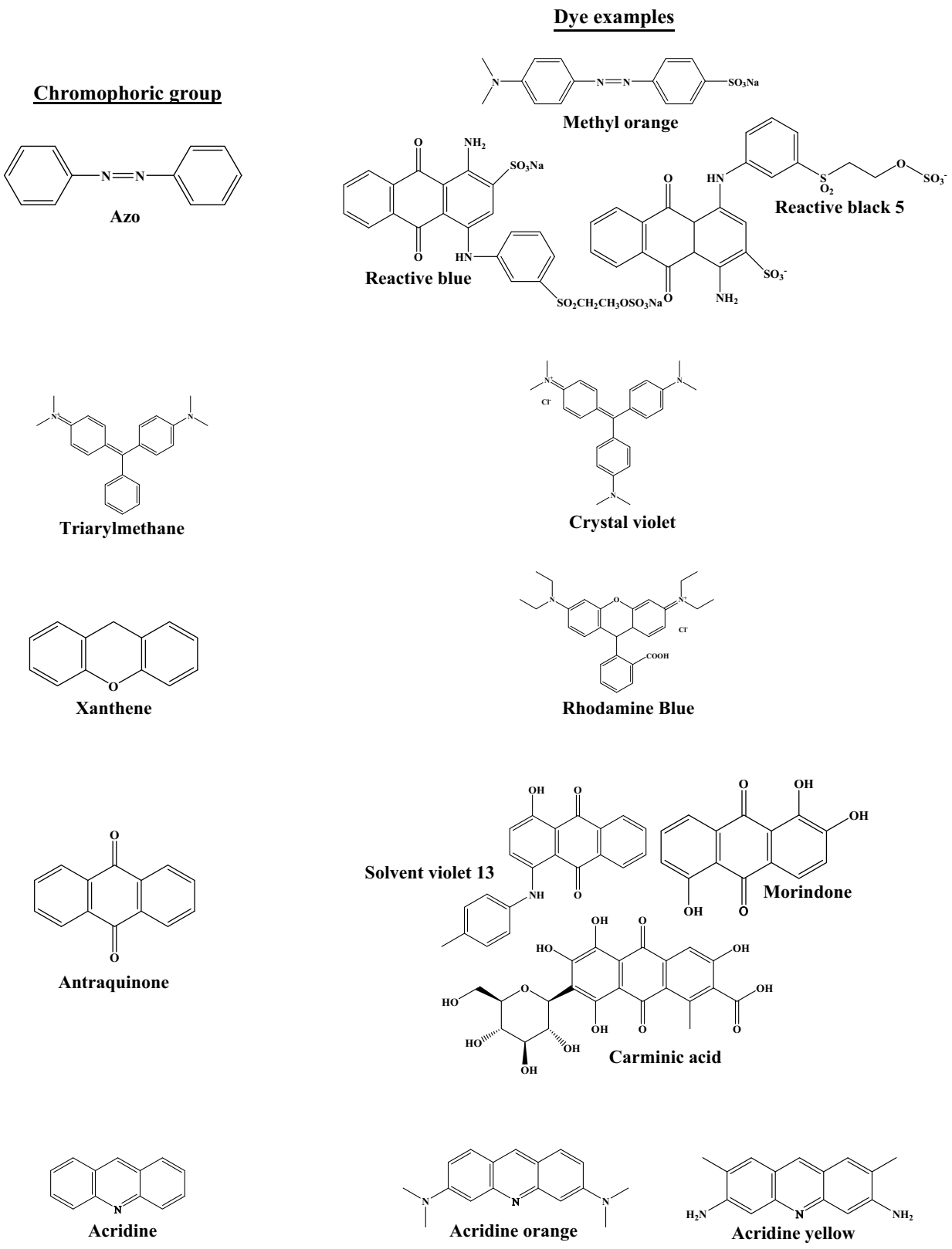

Fig. (9). Chromophoric groups and its dye compound.

CONCLUSION

Iron oxide is an excellent semiconductor that possesses low band gap, wide availability, is highly reactive and non-toxic. Iron oxide was able to successfully activate under visible light radiation. Iron oxide photocatalyst/adsorbent catalytic efficiency is highly dependent on operative parameter such as morphological properties, pH solution, catalyst loading and contact time. The pollutant removal ability of iron

oxide as a parent or modified photocatalyst/adsorbent also demonstrates removal efficiency where high OH yield is produced during the photocatalysis process. The superparamagnetism has shown that they can be recycled and reused for several degradation purposes without/insignificantly affecting its photocatalytic activity. In industrial applications point of view, applying external magnetic force for separation processes has shown its disadvantages under circumstances, such as spaces, costs and times. For future prospects, embedding iron oxide catalysts in polymeric membrane or supporting layer as separation unit may contribute bigger impacts in water and wastewater treatment system by means of simultaneous operations of photocatalytic and separation/filtration principles. Further investigation on membrane choices, fabrication methods and other operative parameters should be carried out to ensure the performance of magnetic photocatalyst membranes is similar as in the suspension form.

CONSENT FOR PUBLICATION

Not applicable.

FUNDING

The author is thankful to the Ministry of Higher Education (MOHE) and Universiti Teknologi Malaysia for the research support from grant number R. J090301.7846.4J184 and R.J130000.2409.04G32. The author would also like to acknowledge financial support from Zamalah Scholarship Universiti Teknologi Malaysia, in addition of technical and management support from the Research Management Center (RMC), Universiti Teknologi Malaysia.

CONFLICT OF INTEREST

The authors declare no conflict of interest, financial or otherwise.

ACKNOWLEDGEMENTS

Declared none.

REFERENCES

[1] Saharan, P.; Chaudhary, G.R.; Mehta, S.K.; Umar, A. Removal of water contaminants by iron oxide nanomaterials. *J. Nanosci. Nanotechnol.,* **2014**, *14*(1), 627-643. [http://dx.doi.org/10.1166/jnn.2014.9053] [PMID: 24730287]

[2] Xu, P.; Zeng, G.M.; Huang, D.L.; Feng, C.L.; Hu, S.; Zhao, M.H.; Lai, C.; Wei, Z.; Huang, C.; Xie, G.X.; Liu, Z.F. Use of iron oxide nanomaterials in wastewater treatment: A review. *Sci. Total Environ.,* **2012**, *424*, 1-10. [http://dx.doi.org/10.1016/j.scitotenv.2012.02.023] [PMID: 22391097]

[3] Parkinson, G.S. Iron oxide surfaces. *Surf. Sci. Rep.,* **2016**, *71*, 272-365. [http://dx.doi.org/10.1016/j.surfrep.2016.02.001]

[4] Chirita, M.; Grozescu, I. Fe_2O_3 - Nanoparticles, physical properties and their photochemical and photoelectrochemical applications. *Chem. Bull. Politeh. Univ Timsisoara,* **2009**, *54*, 1-8.

[5] Liu, D.; Li, Z.; Wang, W.; Wang, G. Hematite doped magnetic TiO_2 nanocomposites with improved photocatalytic activity. *J. Alloys Compd.,* **2016**, *654*, 491-497. [http://dx.doi.org/10.1016/j.jallcom.2015.09.140]

[6] Ling, Y.; Lim, S.; Chyuan, H.; Tong, W. Research progress on iron oxide-based magnetic materials: Synthesis techniques and photocatalytic applications. *Ceram. Int.,* **2016**, *42*, 9-34. [http://dx.doi.org/10.1016/j.ceramint.2015.08.144]

[7] Lu, A.H.; Salabas, E.L.; Schüth, F. Magnetic nanoparticles: Synthesis, protection, functionalization, and application. *Angew. Chem. Int. Ed. Engl.,* **2007**, *46*(8), 1222-1244. [http://dx.doi.org/10.1002/anie.200602866] [PMID: 17278160]

[8] Carvalho, M.D.; Henriques, F.; Ferreira, L.P.; Godinho, M.; Cruz, M.M. Iron oxide nanoparticles: The influence of synthesis method and size on composition and magnetic properties. *J. Solid State Chem.,* **2013**, *201*, 144-152. [http://dx.doi.org/10.1016/j.jssc.2013.02.024]

[9] Agiotis, L.; Theodorakos, I.; Samothrakitis, S.; Papazoglou, S.; Zergioti, I.; Raptis, Y.S. Magnetic manipulation of superparamagnetic nanoparticles in a microfluidic system for drug delivery applications. *J. Magn. Magn. Mater.,* **2016**, *401*, 956-964. [http://dx.doi.org/10.1016/j.jmmm.2015.10.111]

[10] Madrakian, T.; Afkhami, A.; Haryani, R.; Ahmadi, M. Synthesis of γ-Fe_2O_3/TiO_2 nanocomposite and its application in removal of dyes from water samples by adsorption and degradation processes. *RSC Adv.,* **2014**, *4*, 44841-44847. [http://dx.doi.org/10.1039/C4RA06421F]

[11] Ergeneman, O.; Peters, C.; Gullo, M.R.; Jacot-Descombes, L.; Gervasoni, S.; Özkale, B.; Fatio, P.; Cadarso, V.J.; Mastrangeli, M.; Pané, S.; Brugger, J.; Hierold, C.; Nelson, B.J. Inkjet printed superparamagnetic polymer composite hemispheres with programmed magnetic anisotropy. *Nanoscale,* **2014**, *6*(18), 10495-10499. [http://dx.doi.org/10.1039/C3NR06442E] [PMID: 24842483]

[12] Damean, N.; Parviz, B.A; Lee, J.N.; Odom, T.; Whitesides, G.M. Composite ferromagnetic photoresist for the fabrication of microelectromechanical systems. *J. Micromech. Microeng.,* **2004**, *15*, 29-34. [http://dx.doi.org/10.1088/0960-1317/15/1/005]

[13] Kim, J.; Chung, S.E.; Choi, S.E.; Lee, H.; Kim, J.; Kwon, S. Programming magnetic anisotropy in polymeric micro-actuators. *Nat. Mater.,* **2011**, *10*(10), 747-752. [http://dx.doi.org/10.1038/nmat3090] [PMID: 21822261]

[14] Ye, F.; Ohmori, A.; Li, C. New approach to enhance the photocatalytic activity of plasma sprayed TiO_2 coatings using P-N junctions. *Surf. Coat. Tech.,* **2004**, *184*, 233-238. [http://dx.doi.org/10.1016/j.surfcoat.2003.11.012]

[15] Bhatkhande, D.S.; Pangarkar, V.G.; Beenackers, A.A.C.M. Photocatalytic degradation for environmental applications. A review. *J. Chem. Technol. Biotechnol.,* **2002**, *77*, 102-116. [http://dx.doi.org/10.1002/jctb.532]

[16] Mobtaker, H.G.; Ahmadi, S.J.; Ashtari, P. Nano-TiO_2/Nd deposited on γ-Fe_2O_3 as a magnetically separable photocatalyst. *J. Sci.,* **2014**, *25*, 281-285.

[17] Lin, Y.; Geng, Z.; Cai, H.; Ma, L.; Chen, J.; Zeng, J.; Pan, N.; Wang, X. c. *Eur. J. Inorg. Chem.,* **2012**, *2012*(28), 4439-4444. [http://dx.doi.org/10.1002/ejic.201200454]

[18] Tan, L.; Zhang, X.; Liu, Q.; Jing, X.; Liu, J.; Song, D.; Hu, S.; Liu, L.; Wang, J. Synthesis of Fe_3O_4@TiO_2 core-shell magnetic composites for highly efficient sorption of Uranium (VI). *Colloids Surf. A Physicochem. Eng. Asp.,* **2015**, *469*, 279-286. [http://dx.doi.org/10.1016/j.colsurfa.2015.01.040]

[19] Mishra, M.F.; Chun, D. M. α-Fe_2O_3 as a photocatalytic material: A review. *Appl. Catal. A Gen.,* **2015**, *498*, 126-141. [http://dx.doi.org/10.1016/j.apcata.2015.03.023]

[20] Chen, Y.H.; Lin, C.C. Effect of nano-hematite morphology on photocatalytic activity. *Phys. Chem. Miner.,* **2014**, *41*, 727-736. [http://dx.doi.org/10.1007/s00269-014-0686-9]

[21] Li, L.; Wang, M. Advanced nanomatericals for solar photocatalysis. In: Advanced Catalytic Materials - Photocatalysis and Other Current Trends*;* Norena, L.E.; Wang, J.A., Eds.; In: Tech, **2016**, pp. 169-230. [http://dx.doi.org/10.5772/62206]

[22] Sajjadi, S.H.; Goharshadi, E.K. Highly monodispersed hematite cubes for removal of ionic dyes. *Biochem. Pharmacol.,* **2017**.

[23] Dafare, S.; Deshpande, P.S.; Bhavsar, R.S. Photocatalytic degradation of Congo Red dye on combustion synthesised Fe_2O_3. *Indian J. Chem. Technol.,* **2013**, *20*, 406-410.

[24] Zhu, Y.; Li, G.; Zhang, Q.; Tang, C. The photocatalytic degradation of methylene blue wastewater with nanoscale ferric oxide as catalyst. *Adv. Mat. Res.,* **2012**, *356-360*, 1813-1818.

[25] Iram, M.; Guo, C.; Guan, Y.; Ishfaq, A.; Liu, H. Adsorption and magnetic removal of neutral red dye from aqueous solution using Fe_3O_4 hollow nanospheres. *J. Hazard. Mater.,* **2010**, *181*(1-3),

1039-1050.
[http://dx.doi.org/10.1016/j.jhazmat.2010.05.119] [PMID: 20566240]

[26] Du, W.; Xu, Y.; Wang, Y. Photoinduced degradation of orange II on different iron (hydr)oxides in aqueous suspension: Rate enhancement on addition of hydrogen peroxide, silver nitrate, and sodium fluoride. *Langmuir,* **2008**, *24*(1), 175-181.
[http://dx.doi.org/10.1021/la7021165] [PMID: 18052220]

[27] Joya, M.R.; Baron-Jaimez, J.; Barba-Ortega, J. Preparation and characterization of Fe_2O_3 nanoparticles. In: *Journal of Physics: Conference Series*, *IOP Publishing*, **2013**, Vol. *466*, No. 1, p. 012004.

[28] Pawar, M.J.; Khajone, A.D. Photodegradation of malachite green dye over sol-gel synthesized nanocrystalline α-Fe_2O_3. *J. Chem. Pharm. Res.,* **2012**, *4*, 1880-1884.

[29] Tadic, M.; Panjan, M.; Damnjanovic, V.; Milosevic, I. Magnetic properties of hematite (Fe_2O_3) nanoparticles prepared by hydrothermal synthesis method. *Appl. Surf. Sci.,* **2014**, *320*, 183-187.
[http://dx.doi.org/10.1016/j.apsusc.2014.08.193]

[30] Kumar, S.; Navjeet, K.Æ. Photocatalytic degradation of two commercial reactive dyes in aqueous phase using nanophotocatalysts. *Nanoscale Res. Lett*., **2009**, *4*, 709-716.

[31] Wang, D.; Guan, K.; Bai, Z.; Liu, F. Facile preparation of acid-resistant magnetite particles for removal of Sb(III) from strong acidic solution. *Sci. Technol. Adv. Mater.,* **2016**, *17*(1), 80-88.
[http://dx.doi.org/10.1080/14686996.2016.1145530] [PMID: 27877860]

[32] Tajabadi, M.; Khosroshahi, M.E. Effect of alkaline media concentration and modification of temperature on magnetite synthesis method using. *Int. J. Chem. Eng. Appl.,* **2012**, *3*, 3-7.
[http://dx.doi.org/10.7763/IJCEA.2012.V3.187]

[33] Thiruvenkatachari, R.; Vigneswaran, S.; Moon, I.S. A review on UV/TiO_2 photocatalytic oxidation process. *Korean J. Chem. Eng.,* **2008**, *25*, 64-72.
[http://dx.doi.org/10.1007/s11814-008-0011-8]

[34] Khedr, M.H.; Halim, K.S.A.; Soliman, N.K. Synthesis and photocatalytic activity of nano-sized iron oxides. *Mater. Lett.,* **2009**, *63*, 598-601.
[http://dx.doi.org/10.1016/j.matlet.2008.11.050]

[35] Pinna, N.; Grancharov, S.; Beato, P.; Bonville, P.; Antonietti, M.; Niederberger, M. Magnetite nanocrystals: Nonaqueous synthesis, characterization, and solubility. *Chem. Mater.,* **2005**, *17*, 3044-3049.
[http://dx.doi.org/10.1021/cm050060+]

[36] Shahpari, M.; Behjat, A.; Khajaminian, M.; Torabi, N. The influence of morphology of hematite (α-Fe_2O_3) counter electrodes on the efficiency of dye-sensitized solar cells. *Sol. Energ.,* **2015**, *119*, 45-53.
[http://dx.doi.org/10.1016/j.solener.2015.06.039]

[37] He, Y.T.; Wan, J.; Tokunaga, T. Kinetic stability of hematite nanoparticles: The effect of particle sizes. *J. Nanopart. Res.,* **2008**, *10*, 321-332.
[http://dx.doi.org/10.1007/s11051-007-9255-1]

[38] Baalousha, M. Aggregation and disaggregation of iron oxide nanoparticles: Influence of particle concentration, pH and natural organic matter. *Sci. Total Environ.,* **2009**, *407*(6), 2093-2101.
[http://dx.doi.org/10.1016/j.scitotenv.2008.11.022] [PMID: 19059631]

[39] Liu, G.; Deng, Q.; Yang, Y.; Wang, H.M.; Wang, G.Z. Micro/nanostructured α-Fe_2O_3 with structural enhanced removal capacity of Cr(VI). *Ions. Adv. Mater. Res.,* **2012**, *518*, 1753-1756.

[40] Liu, G.; Deng, Q.; Wang, H.; Ng, D.H.L.; Kong, M.; Cai, W.; Wang, G. Micro/nanostructured α-Fe_2O_3 spheres: Synthesis, characterization, and structurally enhanced visible-light photocatalytic activity. *J. Mater. Chem.,* **2012**, *22*, 9704.
[http://dx.doi.org/10.1039/c2jm31586f]

[41] Zhou, X.; Lan, J.; Liu, G.; Deng, K.; Yang, Y.; Nie, G.; Yu, J.; Zhi, L. Facet-mediated photodegradation of organic dye over hematite architectures by visible light. *Angew. Chem. Int. Ed. Engl.,* **2012**, *51*(1), 178-182.
[http://dx.doi.org/10.1002/anie.201105028] [PMID: 22086657]

[42] Liu, Y.; Yu, C.; Dai, W.; Gao, X.; Qian, H.; Hu, Y.; Hu, X. One-pot solvothermal synthesis of multi-shelled α-Fe_2O_3 hollow spheres with enhanced visible-light photocatalytic activity. *J. Alloys Compd.,* **2013**, *551*, 440-443.
[http://dx.doi.org/10.1016/j.jallcom.2012.11.047]

[43] Cha, H.G.; Kim, S.J.; Lee, K.J.; Jung, M.H.; Kang, Y.S. Single-crystalline porous hematite nanorods: Photocatalytic and magnetic properties. *J. Phys. Chem. C,* **2011**, *115*, 19129-19135.
[http://dx.doi.org/10.1021/jp206958g]

[44] Ahmmad, B.; Leonard, K.; Shariful Islam, M.; Kurawaki, J.; Muruganandham, M.; Ohkubo, T.; Kuroda, Y. Green synthesis of mesoporous hematite (α-Fe_2O_3) nanoparticles and their photocatalytic activity. *Adv. Powder Technol.,* **2012**, *24*, 160-167.
[http://dx.doi.org/10.1016/j.apt.2012.04.005]

[45] Mondal, K.; Sharma, A. Photocatalytic oxidation of pollutant dyes in wastewater by TiO_2 and ZnO nano-materials-A mini-review. *Indian Inst. Tecnol.,* **2016**, pp. 36-72.

[46] Liu, Y.; Yu, H.; Zhan, S.; Li, Y.; Lv, Z.; Yang, X.; Yu, Y. Fast degradation of methylene blue with electrospun hierarchical α-Fe_2O_3 nanostructured fibers. *J. Sol-Gel Sci. Technol.,* **2011**, *58*, 716-723.
[http://dx.doi.org/10.1007/s10971-011-2451-6]

[47] Dang, S.N.; Lu, S.X.; Xu, W.G.; Sa, J. Dark-degradation of reactive brilliant blue X-BR in aqueous solution using α-Fe_2O_3. *J. Non-Cryst. Solids,* **2008**, *354*, 5018-5021.
[http://dx.doi.org/10.1016/j.jnoncrysol.2008.07.027]

[48] Al-Anbari, R.; Al-obaidy, A.H.; Abd, E. Photocatalytic activity of Fe_3O_4 under solar radiation. *Mesopotamia Environ. J.,* **2016**, *2*, 41-53.

[49] El-Latif, M.M.A.; Ibrahim, A.M.; Showman, M.S.; Hamide, R.R.A. Alumina/iron oxide nano composite for cadmium ions removal from aqueous solutions. *Int. J. Nonferrous Metall.,* **2013**, *2013*, 47-62.
[http://dx.doi.org/10.4236/ijnm.2013.22007]

[50] Fan, F.L.; Qin, Z.; Bai, J.; Rong, W.D.; Fan, F.Y.; Tian, W.; Wu, X.L.; Wang, Y.; Zhao, L. Rapid removal of uranium from aqueous solutions using magnetic Fe_3O_4@SiO_2 composite particles. *J. Environ. Radioact.,* **2012**, *106*, 40-46.
[http://dx.doi.org/10.1016/j.jenvrad.2011.11.003] [PMID: 22304999]

[51] Zhang, Y.U.; Yang, M.I.N.; Dou, X. Arsenate Adsorption on an Fe - Ce Bimetal Oxide Adsorbent: Role of Surface Properties. *Environ. Sci. Technol*, **2005**, *39*, 7246-7253.

[52] Konstantinou, I.K.; Albanis, T.A. TiO_2-assisted photocatalytic degradation of azo dyes in aqueous solution: Kinetic and mechanistic investigations. A review. *Appl. Catal. B,* **2004**, *49*, 1-14.
[http://dx.doi.org/10.1016/j.apcatb.2003.11.010]

[53] Ahmed, S.; Rasul, M.G.; Brown, R.; Hashib, M.A. Influence of parameters on the heterogeneous photocatalytic degradation of pesticides and phenolic contaminants in wastewater: A short review. *J. Environ. Manag.,* **2011**, *92*(3), 311-330.
[http://dx.doi.org/10.1016/j.jenvman.2010.08.028] [PMID: 20950926]

[54] Shirivastava, D.S.S.V.S. Adsorptive removal of heavy metals by magnetic nanoadsorbent: An equilibrium and thermodynamic study. *Appl. Nanosci.,* **2015**, *5*, 927-935.
[http://dx.doi.org/10.1007/s13204-014-0390-6]

[55] Hashem, S.; Parsafar, G.; Goharshadi, E.K. Kinetics study of removal of reactive black 5 from aqueous solutions using hematite nanoparticles fabricated by hydrothermal method. **2012**, 12-14.

[56] Yoon, S.U.; Mahanty, B.; Ha, H.M.; Kim, C.G. Phenol adsorption on surface-functionalized iron oxide nanoparticles: Modeling of the kinetics, isotherm, and mechanism. *J. Nanopart. Res.,* **2016**, 18(6), 170.
[http://dx.doi.org/10.1007/s11051-016-3478-y]

[57] Lassoued, A.; Saber, M.; Brahim, L.; Salah, D.; Abdellatif, A. Photocatalytic degradation of methylene blue dye by iron oxide (α-Fe_2O_3) nanoparticles under visible irradiation. *J. Mater. Sci. Mater. Electron.,* **2018**, 29(10), 8142-8152.
[http://dx.doi.org/10.1007/s10854-018-8819-4]

[58] Momeni, M.M. Influence of top morphology of hematite nanotubes on photo degradation of methylene blue and solar water splitting performance influence of top morphology of hematite nanotubes on photo degradation of methylene blue and solar water splitting performance. *Mater. Res. Innov.,* **2016**, 20(5), 390-394.

[59] Gandha, K.; Mohapatra, J.; Hossain, M.K.; Elkins, K.; Poudyal, N.; Rajeshwar, K.; Liu, J.P. Mesoporous iron oxide nanowires: Synthesis, magnetic and photocatalytic properties. *RSC Adv.,* **2016**, *6*, 90537-90546.
[http://dx.doi.org/10.1039/C6RA18530D]

[60] Huang, Y.; Ding, D.; Zhu, M.; Meng, W.; Huang, Y.; Geng, F.; Li,

J.; Lin, J.; Tang, C.; Lei, Z.; Zhang, Z.; Zhi, C. Facile synthesis of α-Fe_2O_3 nanodisk with superior photocatalytic performance and mechanism insight. *Sci. Technol. Adv. Mater.,* **2015**, *16*(1) 014801 [http://dx.doi.org/10.1088/1468-6996/16/1/014801] [PMID: 27877744]

[61] Ayachi, A.A.; Mechakra, H.; Silvan, M.M.; Boudjaadar, S.; Achour, S. Monodisperse α-Fe_2O_3 nanoplatelets: Synthesis and characterization. *Ceram. Int.,* **2015**, *41*, 2228-2233. [http://dx.doi.org/10.1016/j.ceramint.2014.10.024]

[62] Lin, D.; Deng, B.; Sassman, S.A.; Hu, Y.; Cheng, G.J. Magnetic field assisted growth of highly dense α-Fe_2O_3 single crystal nanosheets and their application in water treatment. *RSC Adv.,* **2014**, *4*, 18621-18626. [http://dx.doi.org/10.1039/C3RA47726F]

[63] Xia, J.; Liu, H.; Cheng, X.; Yin, S.; Li, H.; Xu, H.; Xu, L.; Qiu, Y. Reactable ionic liquid synthesis and visible-light photocatalytic activity of dendritic ferric oxide hierarchical structures. *Micro Nano Lett.,* **2012**, *7*, 806-809. [http://dx.doi.org/10.1049/mnl.2012.0474]

[64] Atabaev, T.S. Facile hydrothermal synthesis of flower-like hematite microstructure with high photocatalytic properties. *J. Adv. Ceram.,* **2015**, *4*, 61-64. [http://dx.doi.org/10.1007/s40145-015-0133-5]

[65] Jiao, Y.; Liu, Y.; Qu, F.; Umar, A.; Wu, X. Visible-light-driven photocatalytic properties of simply synthesized α-Iron(III)oxide nanourchins. *J. Colloid Interface Sci.,* **2015**, *451*, 93-100. [http://dx.doi.org/10.1016/j.jcis.2015.03.055] [PMID: 25890117]

[66] Maji, S.K.; Mukherjee, N.; Mondal, A.; Adhikary, B. Synthesis, Characterization and Photocatalytic Activity of α-Fe2O3 Nanoparticles. *Polyhedron*, **2012**, *33*, 145-149.

[67] Fujishima, A.; Zhang, X.; Tryk, D.A. TiO_2 photocatalysis and related surface phenomena. *Surf. Sci. Rep.,* **2008**, *63*, 515-582. [http://dx.doi.org/10.1016/j.surfrep.2008.10.001]

[68] Zuo, R.; Du, G.; Zhang, W.; Liu, L.; Liu, Y.; Mei, L.; Li, Z. Photocatalytic degradation of methylene blue using TiO_2 impregnated diatomite. *Adv. Mater. Sci. Eng.,* **2014**. [http://dx.doi.org/10.1155/2014/170148]

[69] Wu, W.; He, Q.; Jiang, C. Magnetic iron oxide nanoparticles: Synthesis and surface functionalization strategies. *Nanoscale Res. Lett.,* **2008**, *3*(11), 397-415. [http://dx.doi.org/10.1007/s11671-008-9174-9] [PMID: 21749733]

[70] Wu, W.; Wu, Z.; Yu, T.; Jiang, C.; Kim, W.S. Recent progress on magnetic iron oxide nanoparticles: Synthesis, surface functional strategies and biomedical applications. *Sci. Technol. Adv. Mater.,* **2015**, *16*(2), 023501. [http://dx.doi.org/10.1088/1468-6996/16/2/023501] [PMID: 27877761]

[71] Teja, A.S.; Koh, P. Synthesis, properties, and applications of magnetic iron oxide nanoparticles. *Prog. Cryst. Growth Charact. Mater.,* **2009**, *55*, 22-45. [http://dx.doi.org/10.1016/j.pcrysgrow.2008.08.003]

[72] Litter, I.; Blesa, M.A. Photodissolution of iron oxides IV. A comparative study on the photodissolution of hematite, magnetite, and maghemite in EDTA media. *Can. J. Chem.,* **1992**, *70*, 2502-2510. [http://dx.doi.org/10.1139/v92-316]

[73] Litter, M.I.; Baumgartner, E.C.; Urrutla, G.A.; Blesa, M.A. Photodissolution of iron oxides. 3. interplay of photochemical and thermal processes in maghemite/carboxylic acid systems. *Environ. Sci. Technol.,* **1991**, *25*, 1907-1913. [http://dx.doi.org/10.1021/es00023a011]

[74] Luan, P.; Xie, M.; Liu, D.; Fu, X.; Jing, L. Effective charge separation in the rutile TiO_2 nanorod-coupled α-Fe_2O_3 with exceptionally high visible activities. *Sci. Rep.,* **2014**, *4*, 6180. [http://dx.doi.org/10.1038/srep06180] [PMID: 25154460]

[75] Xia, Y.; Yin, L. Core-shell structured α-Fe_2O_3@TiO_2 nanocomposites with improved photocatalytic activity in the visible light region. *Phys. Chem. Chem. Phys.,* **2013**, *15*(42), 18627-18634. [http://dx.doi.org/10.1039/c3cp53178c] [PMID: 24085286]

[76] Lee, S.C.; Lintang, H.O.; Yuliati, L. High photocatalytic activity of Fe_2O_3/TiO_2 nanocomposites prepared by photodeposition for degradation of 2,4-dichlorophenoxyacetic acid. *Beilstein J. Nanotechnol.,* **2017**, *8*, 915-926. [http://dx.doi.org/10.3762/bjnano.8.93] [PMID: 28546886]

[77] Yu, X.X.; Dong, F.Z.; Dong, B.; Liu, L.; Wu, Y. High visible-light photocatalytic performance of natural hematite ore composited with ZnO nanomaterials. *Adv. Mater. Lett.,* **2017**, *8*, 393-397. [http://dx.doi.org/10.5185/amlett.2017.7079]

[78] Suresh, R.; Sandoval, C.; Ramirez, E.; Alverez, A.; Mansilla, D.H.; Mangalaraja, R.V.; Yanez, J. Solid-state synthesis and characterization of α-Fe_2O_3@ZnO nanocomposites with enhanced visible light driven photocatalytic activity. *J. Mater. Sci. Mater. Electron.,* **2018**, *29*, 20347-20355. [http://dx.doi.org/10.1007/s10854-018-0170-2]

[79] Abdullah Mirzaie, R.; Kamrani, F.; Anaraki Firooz, A.; Khodadadi, A.A. Effect of α-Fe_2O_3 addition on the morphological, optical and decolorization properties of ZnO nanostructures. *Mater. Chem. Phys.,* **2012**, *133*, 311-316. [http://dx.doi.org/10.1016/j.matchemphys.2012.01.029]

[80] Xi, G.; Yue, B.; Cao, J.; Ye, J. Fe_3O_4/WO_3 hierarchical core-shell structure: High-performance and recyclable visible-light photocatalysis. *Chemistry,* **2011**, *17*(18), 5145-5154. [http://dx.doi.org/10.1002/chem.201002229] [PMID: 21432916]

[81] Karunakaran, C.; Sakthiraadha, S.; Gomathisankar, P.; Vinayagamoorthy, P. Fe_3O_4/SnO_2 nanocomposite: Hydrothermal and sonochemical synthesis, characterization, and visible-light photocatalytic and bactericidal activities. *Powder Technol.,* **2013**, *246*, 635-642. [http://dx.doi.org/10.1016/j.powtec.2013.06.011]

[82] Wang, C.; Yin, L.; Zhang, L.; Kang, L.; Wang, X.; Gao, R. Magnetic (γ-Fe_2O_3@SiO_2)N@TiO_2 functional hybrid nanoparticles with actived photocatalytic ability. *J. Phys. Chem. C,* **2009**, *113*, 4008-4011. [http://dx.doi.org/10.1021/jp809835a]

[83] Peña-Flores, J.I.; Palomec-Garfias, A.F.; Márquez-Beltrán, C.; Sánchez-Mora, E.; Gómez-Barojas, E.; Pérez-Rodríguez, F. Effect on the optical properties of TiO_2:Fe_2O_3 nanostructured composites supported on SiO_2 microsphere assemblies. Nanoscale Res Lett., **2014**, *9*(1), 499.

[84] Stobinski, L.; Lesiak, B.; Malolepszy, A.; Mazurkiewicz, M.; Mierzwa, B.; Zemek, J.; Jiricek, P.; Bieloshapka, I. Graphene oxide and reduced graphene oxide studied by the XRD. TEM and electron spectroscopy methods. *J. Electron Spectros. Relat. Phenomena,* **2014**, *195*, 145-154. [http://dx.doi.org/10.1016/j.elspec.2014.07.003]

[85] Georgakilas, V.; Tiwari, J.N.; Kemp, K.C.; Perman, J.A.; Bourlinos, A.B.; Kim, K.S.; Zboril, R. Noncovalent functionalization of graphene and graphene oxide for energy materials, biosensing, catalytic, and biomedical applications. *Chem. Rev.,* **2016**, *116*(9), 5464-5519. [http://dx.doi.org/10.1021/acs.chemrev.5b00620] [PMID: 27033639]

[86] Chen, Y.; Yan, Q.; Zhang, S.; Lu, L.; Xie, B.; Xie, T.; Zhang, Y.; Wu, Y.; Zhang, Y.; Liu, D. Buffering agents-assisted synthesis of nitrogen-doped graphene with oxygen-rich functional groups for enhanced electrochemical performance. *J. Power Sources,* **2016**, *333*, 125-133. [http://dx.doi.org/10.1016/j.jpowsour.2016.09.111]

[87] Singh, V.K.; Patra, M.K.; Manoth, M.; Gowd, G.S.; Vadera, S.R.; Kumar, N. *In situ* synthesis of graphene oxide and its composites with iron oxide. *N. Carbon Mater.,* **2009**, *24*, 147-152. [http://dx.doi.org/10.1016/S1872-5805(08)60044-X]

[88] Wang, C.; Salmon, L.; Ciganda, R.; Yate, L.; Moya, S.; Ruiz, J.; Astruc, D. An efficient parts-per-million α-Fe_2O_3 nanocluster/graphene oxide catalyst for Suzuki-Miyaura coupling reactions and 4-nitrophenol reduction in aqueous solution. *Chem. Commun. (Camb.),* **2017**, *53*(3), 644-646. [http://dx.doi.org/10.1039/C6CC08401J] [PMID: 27990528]

[89] Gao W. The chemistry of graphene oxide. In: *Graphene oxide*, Springer, Cham, **2015**, pp. 61-95. [http://dx.doi.org/10.1007/978-3-319-15500-5_3]

[90] Anjaneyulu, R.B.; Mohan, B.S.; Naidu, G.P.; Muralikrishna, R. Visible light enhanced photocatalytic degradation of methylene blue by ternary nanocomposite, MoO_3/Fe_2O_3/rGO. *J. Asian Ceram. Soc.,* **2018**, *6*, 183-195. [http://dx.doi.org/10.1080/21870764.2018.1479011]

[91] Zhang, L.; Bao, Z.; Yu, X.; Dai, P.; Zhu, J.; Wu, M.; Li, G.; Liu, X.; Sun, Z.; Chen, C. Rational design of α-Fe_2O_3/reduced graphene oxide composites: Rapid detection and effective removal of organic pollutants. *ACS Appl. Mater. Interfaces,* **2016**, *8*(10), 6431-6438. [http://dx.doi.org/10.1021/acsami.5b11292] [PMID: 26907977]

[92] Pakuła, M.; Biniak, S.; Swiatkowski, A. Chemical and electrochemical studies of interactions between Iron (III) ions and an activated carbon surface. *Langmuir,* **1998**, *14*, 3082-3089.

[http://dx.doi.org/10.1021/la9705625]

[93] Liu, W.; Zhang, J.; Zhang, C.; Ren, L. Preparation and evaluation of activated carbon-based iron-containing adsorbents for enhanced Cr(VI) removal: Mechanism study. *Chem. Eng. J.,* **2012**, *189-190*, 295-302.
[http://dx.doi.org/10.1016/j.cej.2012.02.082]

[94] Kadirova, Z.C.; Hojamberdiev, M.; Katsumata, K.; Isobe, T.; Matsushita, N.; Nakajima, A.; Okada, K. Fe_2O_3-loaded activated carbon fiber/polymer materials and their photocatalytic activity for methylene blue mineralization by combined heterogeneous-homogeneous photocatalytic processes. *Appl. Surf. Sci.,* **2017**, *402*, 444-455.
[http://dx.doi.org/10.1016/j.apsusc.2017.01.131]

[95] Li, G.; Jiang, Y.; Huang, K.; Ding, P.; Yao, L. Kinetics of adsorption of saccharomyces cerevisiae mandelated dehydrogenase on magnetic Fe_3O_4 - chitosan nanoparticles. *Colloids Surf. A.,* **2008**, *320*, 11-18.

[96] Broujeni, B.R.; Nilchi, A.; Hassani, A.H.; Saberi, R. Preparation and characterization of chitosan/Fe_2O_3 nano composite for the adsorption of thorium (IV) ion from aqueous solution. *Water Sci. Technol.,* **2018**, *78*(3-4), 708-720.
[http://dx.doi.org/10.2166/wst.2018.343] [PMID: 30208011]

[97] Hernández-Alonso, M.D.; Fresno, F.; Suárez, S.; Coronado, J.M. Development of alternative photocatalysts to TiO_2: Challenges and opportunities. *Energy Environ. Sci.,* **2009**, *2*, 1231.
[http://dx.doi.org/10.1039/b907933e]

[98] Yonezawa, T.; Kamoshita, K.; Tanaka, M.; Kinoshita, T. Easy preparation of stable iron oxide nanoparticles using gelatin as stabilizing molecules easy preparation of stable iron oxide nanoparticles using gelatin as stabilizing molecules. *Jpn. J. Appl. Phys.,* **2008**, *47*, 1389-1392.
[http://dx.doi.org/10.1143/JJAP.47.1389]

[99] Gaihre, B.; Aryal, S.; Khil, M.S.; Kim, H.Y. Encapsulation of Fe_3O_4 in gelatin nanoparticles: Effect of different parameters on size and stability of the colloidal dispersion. *J. Microencapsul.,* **2008**, *25*(1), 21-30.
[http://dx.doi.org/10.1080/02652040701737697] [PMID: 18188729]

[100] Andrade, L.; Fabris, D.; Ardisson, D.; Valente, M.A. Effect of tetramethylammonium hydroxide on nucleation, surface modification and growth of magnetic nanoparticles. *J. Nanomater.,* **2012**, *2012*, 1-10.
[http://dx.doi.org/10.1155/2012/454759]

[101] Ankamwar, B.; Lai, T.C.; Huang, J.H.; Liu, R.S.; Hsiao, M.; Chen, C.H.; Hwu, Y.K. Biocompatibility of Fe_3O_4 nanoparticles evaluated by *in vitro* cytotoxicity assays using normal, glia and breast cancer cells. *Nanotechnology,* **2010**, *21*(7), 75102.
[http://dx.doi.org/10.1088/0957-4484/21/7/075102] [PMID: 20090199]

[102] Kontos, A.I.; Likodimos, V.; Stergiopoulos, T.; Tsoukleris, D.S.; Falaras, P.; Rabias, I.; Papavassiliou, G.; Kim, D.; Kunze, J.; Schmuki, P. Self-organized anodic TiO_2 nanotube arrays functionalized by iron oxide nanoparticles. *Chem. Mater.,* **2009**, *21*, 662-672.
[http://dx.doi.org/10.1021/cm802495p]

[103] Harifi, T.; Montazer, M. A robust super-paramagnetic TiO_2:Fe_3O_4:Ag nanocomposite with enhanced photo and bio activities on polyester fabric *via* one step sonosynthesis. *Ultrason. Sonochem.,* **2015**, *27*, 543-551.
[http://dx.doi.org/10.1016/j.ultsonch.2015.04.008] [PMID: 25899439]

[104] Tayefeh, A.; Mousavi, S.A.; Wiesner, M.; Poursalehi, R. Synthesis and surface characterization of magnetite-titania nanoparticles / polyamide nanocomposite smart RO membrane. *Procedia Mater. Sci.,* **2015**, *11*, 342-346.
[http://dx.doi.org/10.1016/j.mspro.2015.11.114]

[105] Yuan, P.; Fan, M.; Yang, D.; He, H.; Liu, D.; Yuan, A.; Zhu, J.; Chen, T. Montmorillonite-supported magnetite nanoparticles for the removal of hexavalent chromium [Cr(VI)] from aqueous solutions. *J. Hazard. Mater.,* **2009**, *166*(2-3), 821-829.
[http://dx.doi.org/10.1016/j.jhazmat.2008.11.083] [PMID: 19135796]

[106] Yang, Y.; Li, X.J.; Chen, J.T.; Wang, L.Y. Effect of doping mode on the photocatalytic activities of Mo/TiO_2. *J. Photochem. Photobiol. Chem.,* **2004**, *163*, 517-522.
[http://dx.doi.org/10.1016/j.jphotochem.2004.02.008]

[107] Li, Y.; Peng, S.; Jiang, F.; Lu, G.; Li, S. Effect of doping TiO_2 with alkaline-earth metal ions on its photocatalytic activity. *J. Serb. Chem. Soc.,* **2007**, *72*, 393-402.
[http://dx.doi.org/10.2298/JSC0704393L]

[108] Guo, J.; Gan, Z.; Lu, Z.; Liu, J.; Xi, J.; Wan, Y.; Le, L.; Liu, H.; Shi, J.; Xiong, R. Improvement of the photocatalytic properties of TiO_2 by (Fe+Mo) Co-doping - A possible way to retard the recombination process. *J. Appl. Phys.,* **2013**, *114*(10), 104903.
[http://dx.doi.org/10.1063/1.4819449]

[109] Sánchez Mora, E.; Gómez Barojas, E.; Rojas Rojas, E.; Silva González, R. Morphological, optical and photocatalytic properties of TiO_2-Fe_2O_3 multilayers. *Sol. Energy Mater. Sol. Cells,* **2007**, *91*, 1412-1415.
[http://dx.doi.org/10.1016/j.solmat.2007.05.010]

[110] Tada, H.; Jin, Q.; Iwaszuk, A.; Nolan, M. Molecular-scale transition metal oxide nanocluster surface- modified titanium dioxide as solar-activated environmental catalysts. *J. Phys. Chem. C,* **2014**, *118*(23), 12077-12086.
[http://dx.doi.org/10.1021/jp412312m]

[111] Thongsuwan, W.; Singjai, P. Influence of TiO_2/Fe_2O_3 interfacial layers on optical properties under visible light. *Surf. Coat. Tech.,* **2015**, *306*, 49-53.
[http://dx.doi.org/10.1016/j.surfcoat.2016.04.026]

[112] Xie, J.; Zhou, Z.; Lian, Y.; Hao, Y.; Li, P.; Wei, Y. Synthesis of α-Fe_2O_3/ZnO composites for photocatalytic degradation of pentachlorophenol under UV-Vis light irradiation. *Ceram. Int.,* **2015**, *41*, 2622-2625.
[http://dx.doi.org/10.1016/j.ceramint.2014.10.043]

[113] Balu, S.; Velmurugan, S.; Palanisamy, S.; Chen, S. Synthesis of α-Fe_2O_3 decorated G-C_3N/ZnO ternary Z-scheme photocatalyst for degradation of tartrazine dye in aqueous media. *J. Taiwan Inst. Chem. Eng.,* **2019**, *9*, 258-267.

[114] Kar, P.; Jain, P.; Kumar, V.; Kumar, R. Interfacial engineering of Fe_2O_3@BOC heterojunction for efficient detoxification of toxic metal and dye under visible light illumination. *J. Environ. Chem. Eng.,* **2019**, *7*(1), 102843.
[http://dx.doi.org/10.1016/j.jece.2018.102843]

[115] Abhilash, M.R.; Akshatha, G.; Srikantaswamy, S. Photocatalytic dye degradation and biological activities of the Fe_2O_3/Cu_2O nanocomposite†. *RSC Adv.,* **2019**, *9*, 8557-8568.
[http://dx.doi.org/10.1039/C8RA09929D]

[116] Lubis, S. Synthesis, characterization and photocatalytic activity of α-Fe_2O_3/bentonite composite prepared by mechanical milling. In: *Journal of Physics: Conference Series*, *IOP Publishing*, **2018**, Vol. *1116*, No. *4*, p. 042016.

[117] Lei, R.; Ni, H.; Chen, R.; Gu, H.; Zhang, B.; Zhan, W. Hydrothermal synthesis of CdS nanorods anchored on α-Fe_2O_3 nanotube arrays with enhanced visible-light-driven photocatalytic properties. *J. Colloid Interface Sci.,* **2018**, *514*, 496-506.
[PMID: 29289732]

[118] Bhatnagar, A.; Sillanpää, M. Removal of Natural Organic Matter (NOM) and its constituents from water by adsorption - A review. *Chemosphere,* **2017**, *166*, 497-510.
[http://dx.doi.org/10.1016/j.chemosphere.2016.09.098] [PMID: 27710885]

[119] Dong, H.; Zeng, G.; Tang, L.; Fan, C.; Zhang, C.; He, X.; He, Y. An overview on limitations of TiO_2-based particles for photocatalytic degradation of organic pollutants and the corresponding countermeasures. *Water Res.,* **2015**, *79*, 128-146.
[http://dx.doi.org/10.1016/j.watres.2015.04.038] [PMID: 25980914]

[120] Anku, W.W.; Mamo, M.A.; Govender, P.P. Phenolic compounds compounds in water: water: sources, phenolic. *Phenolic Compound - Natural Sources, Importance and Application,* **2017**, pp. 419-443.

[121] Oliveira, C.; Lima, D.L.D.; Silva, C.P.; Otero, M.; Esteves, V.I. Photodegradation behaviour of estriol: An insight on natural aquatic organic matter influence. *Chemosphere,* **2016**, *159*, 545-551.
[http://dx.doi.org/10.1016/j.chemosphere.2016.06.046] [PMID: 27341158]

[122] Pulgarin, C.; Kiwi, J. Iron oxide-mediated degradation, photodegradation, and biodegradation of aminophenols. *Langmuir,* **1995**, *11*, 519-526.
[http://dx.doi.org/10.1021/la00002a026]

[123] Gaffour, H.; Mokhtari, M. Photocatalytic degradation of 4-nitrophenol using TiO_2+Fe_2O_3 and TiO_2/Fe_2O_3-supported bentonite as heterogeneous catalysts. *Res. Chem. Intermed.,* **2016**, *42*(6),

6025-6038.
[http://dx.doi.org/10.1007/s11164-016-2436-8]

[124] Smith, A.H.; Lopipero, P.A.; Bates, M.N.; Steinmaus, C.M. *Arsenic Epidemiology and Drinking Water Standards*. Science's Compass, **2002**, pp. 2145-2146.

[125] Mayo, J.T.; Yavuz, C.; Yean, S.; Cong, L.; Shipley, H.; Yu, W.; Falkner, J.; Kan, A. The effect of nanocrystalline magnetite size on arsenic removal. *Sci. Technol. Adv. Mater.,* **2007**, *8*, 71-75.
[http://dx.doi.org/10.1016/j.stam.2006.10.005]

[126] Yu, L.; Peng, X.; Ni, F.; Li, J.; Wang, D.; Luan, Z. Arsenite removal from aqueous solutions by γ-Fe_2O_3-TiO_2 magnetic nanoparticles through simultaneous photocatalytic oxidation and adsorption. *J. Hazard. Mater.,* **2013**, *246-247*, 10-17.
[http://dx.doi.org/10.1016/j.jhazmat.2012.12.007] [PMID: 23276789]

[127] Zhong, B.L.; Hu, J.; Liang, H.; Cao, A.; Song, W.; Wan, L. Self-assembled 3D flowerlike iron oxide nanostructures and their application in water treatment. *Adv. Mater.,* **2006**, *18*, 2426-2431.
[http://dx.doi.org/10.1002/adma.200600504]

[128] Idris, A.; Hassan, N.; Mohd Ismail, N.S.; Misran, E.; Yusof, N.M.; Ngomsik, A.F.; Bee, A.; Bee, A. Photocatalytic magnetic separable beads for chromium (VI) reduction. *Water Res.,* **2010**, *44*(6), 1683-1688.
[http://dx.doi.org/10.1016/j.watres.2009.11.026] [PMID: 19963234]

[129] Gupta, V.K.; Agarwal, S.; Saleh, T.A. Chromium removal by combining the magnetic properties of iron oxide with adsorption properties of carbon nanotubes. *Water Res.,* **2011**, *45*(6), 2207-2212.
[http://dx.doi.org/10.1016/j.watres.2011.01.012] [PMID: 21303713]

[130] Hu, H.; Wang, Z.; Pan, L. Synthesis of monodisperse Fe_3O_4@silica core – shell microspheres and their application for removal of heavy metal ions from water. *J. Alloys Compd.,* **2010**, *492*, 656-661.
[http://dx.doi.org/10.1016/j.jallcom.2009.11.204]

[131] Mohamed, T.; Attia, S.; Hu, X.L.; Yin, D.Q. Synthesised Magnetic Nanoparticles Coated Zeolite (MNCZ) for the removal of arsenic (As) from aqueous solution. *J. Exp. Nanosci.,* **2014**, *9*(6), 551-560.

[132] Es, B. Photocatalytic removal of Pb ions from aqueous solution using Fe_2O_3 doped in G-C_3N_4 nanocomposite under visible light. *Front. Nanosci. Nanotechnol.,* **2016**, *2*, 100-106.
[http://dx.doi.org/10.15761/FNN.1000116]

[133] Al-farhan, B.S. Removal of Cd^{+2} and Pb^{+2} ions from aqueous solutions using bentonite-modified magnetic nanoparticles. *Int. J. Nanomater. Chem.,* **2016**, *2*, 27-31.
[http://dx.doi.org/10.18576/ijnc/020105]

[134] Zhu, H.; Fu, Y.; Jiang, R.; Yao, J.; Xiao, L.; Zeng, G. Optimization of Copper (II) adsorption onto novel magnetic calcium alginate / maghemite hydrogel beads using response surface methodology. *Ind. Eng. Chem. Res.,* **2014**, *10*, 4059-4066.
[http://dx.doi.org/10.1021/ie4031677]

[135] Vélez, E.; Campillo, G.E.; Morales, G.; Hincapié, C.; Osorio, J.; Arnache, O.; Uribe, J.I.; Jaramillo, F. Mercury removal in wastewater by iron oxide nanoparticles. *J. Phys. Conf. Ser.,* **2016**, *687*, 4.
[http://dx.doi.org/10.1088/1742-6596/687/1/012050]

[136] Asl, M.I.; Ghazi, M.M.; Jahangiri, M. Synthesis, characterization and degradation activity of methyl orange azo dye using synthesized CuO/α-Fe_2O_3 nanocomposite. *Adv. Environ. Technol.,* **2016**, *3*, 143-151.

[137] Ng, T.W.; Zhang, L.; Liu, J.; Huang, G.; Wang, W.; Wong, P.K. Visible-light-driven photocatalytic inactivation of *Escherichia coli* by magnetic Fe_2O_3-AgBr. *Water Res.,* **2016**, *90*, 111-118.
[http://dx.doi.org/10.1016/j.watres.2015.12.022] [PMID: 26724445]

[138] Ma, S.; Zhan, S.; Jia, Y.; Zhou, Q. Superior antibacterial activity of Fe_3O_4-TiO_2 nanosheets under Solar Light. *ACS Appl. Mater. Interfaces,* **2015**, *7*(39), 21875-21883.
[http://dx.doi.org/10.1021/acsami.5b06264] [PMID: 26372171]